Actin binding domain of Rng2 sparsely bound on F-actin strongly inhibits actin movement on myosin II

Running title: Rng2CHD inhibits actomyosin II movement

Yuuki Hayakawa[1, 6], Masak Takaine[2, 6, #], Kien Xuan Ngo[3,6], Taiga Imai[4], Masafumi D. Yamada[5], Arash Badami Behjat[3], Kenichi Umeda[3], Keiko Hirose[2, 5], Ayhan Yurtsever[3], Noriyuki Kodera[3], Kiyotaka Tokuraku[4], Osamu Numata[2], Takeshi Fukuma[3], Toshio Ando[3], Kentaro Nakano[2,*], Taro Q.P. Uyeda[1, 2, 5,*]

[1] Department of Physics, Faculty of Science and Engineering, Graduate School of Waseda University, Shinjuku, Tokyo 169-8555, Japan

[2] Department of Biology, Degree Programs in Life and Earth Sciences, Graduate School of Science and Technology, University of Tsukuba, Tsukuba, Ibaraki 305-8572, Japan

[3] Nano Life Science Institute (WPI-NanoLSI), Kanazawa University, Kanazawa, Ishikawa 920-1192, Japan

[4] Department of Applied Sciences, Muroran Institute of Technology, Muroran, Hokkaido 050-8585, Japan

[5] Biomedical Research Institute, National Institute of Advanced Industrial Science and Technology, Tsukuba, Ibaraki 305-8565, Japan

[6] These authors contributed equally.

[#]Present addresses: Gunma University Initiative for Advanced Research (GIAR) and Institute for Molecular and Cellular Regulation (IMCR), Gunma University, Maebashi 371-8512, Japan

[*] Correspondence: t-uyeda@waseda.jp and knakano@biol.tsukuba.ac.jp

Abstract

Substoichiometric binding of certain actin-binding proteins induces conformational changes in a disproportionally large number of actin protomers in actin filaments. Here, we report a case in which such conformational changes in actin filaments have profound functional consequences. Rng2 is an IQGAP protein implicated in the assembly and contraction of contractile rings in *Schizosaccharomyces pombe*. We found that the calponin-homology actin-binding domain of Rng2 (Rng2CHD) strongly inhibits the motility of actin filaments on myosin II *in vitro.* On skeletal muscle myosin II-coated surfaces, Rng2CHD halved the sliding speed of actin filaments at a binding ratio of 1.3% (=1/77), and virtually stopped movement at a binding ratio of 11% (=1/9). Rng2CHD also inhibited actin movements on *Dictyostelium* myosin II, but in this case by inducing the detachment of actin filaments from myosin II-coated surfaces. Rng2CHD induced cooperative structural changes of actin filaments accompanied by shortening of the filament helical pitch, and reduced the affinity between actin filaments and subfragment 1 (S1) of muscle myosin II in the presence of ADP. Intriguingly, actin-activated ATPase of S1 was hardly inhibited by Rng2CHD. We suggest that sparsely bound Rng2CHD induces global structural changes of actin filaments and interferes with the force generation by actin-myosin II.

Introduction

Actin exists in all eukaryotic cells and performs a wide variety of functions. The interaction between actin and myosin II drives a variety of motile activities such as muscle contraction (Huxley and Niedergerke, 1954; Huxley and Hanson, 1954), the amoeboid movement of cells (Pollard et al., 1974; Clarke and Spudich, 1977; Korn, 1978), and the contraction of contractile rings (CRs). A CR is a ring-like structure that appears transiently on the equatorial plane underneath the cell membrane during cytokinesis of animal cells and many unicellular eukaryotes (Pollard, 2010). A CR consists of actin filaments and myosin II filaments, together with a number of actin-binding proteins (ABPs). It is thought that a CR contracts by sliding between the two filament systems due to actomyosin movement (Mabuchi and Okuno, 1977; Satterwhite and Pollard, 1992). The mechanism of assembly/disassembly of CRs, as well as the mechanism by which contraction is regulated, have been subjected to extensive research, and recent advances using various model organisms, particularly the fission yeast *Schizosaccharomyces pombe*, have established the roles of major factors in these processes (Goyal et al., 2011). However, CRs are under elaborate spatiotemporal control involving a plethora of ABPs and other regulatory proteins, and our understanding of their functions is far from complete.

One such yet incompletely characterized CR-related ABP is Rng2 in *S. pombe*. Rng2 is an IQ motif-containing GTPase activating protein (IQGAP) that plays important roles in the formation of CRs (Eng et al., 1998; Takaine et al., 2009). It is believed that Rng2 crosslinks and bundles actin filaments together to form CRs because only abnormal accumulation of actin filaments was observed at their division sites in Rng2 knockout *S. pombe* cells and in temperature-sensitive Rng2 mutant cells at a restrictive temperature (Eng et al., 1998; Takaine et al., 2009). Additionally, temperature-sensitive Rng2 mutant cells showed normal actin filament rings at the permissive temperature but the distribution of myosin II on actin filaments was abnormal (Takaine et al., 2009). This latter result suggests that Rng2 regulates the interaction between actin filaments and myosin II filaments. Therefore, we have been investigating if Rng2CHD, a 181 amino acid residue-long calponin-homology actin binding domain (CHD) at the N-terminus of Rng2, exhibits *in vitro* activities that are related to the regulation of assembly and/or contraction of CRs.

To our surprise, we found that Rng2CHD inhibits, rather than promotes, actomyosin motility during *in vitro* motility assays in which actin filaments move on surfaces coated with skeletal muscle myosin II or *Dictyostelium* non-muscle myosin II. We investigated the mechanism of inhibition using muscle myosin II, which was more strongly inhibited by Rng2CHD. We found that Rng2CHD bound on actin filaments strongly inhibited actomyosin II motility even when binding was sparse, without significantly inhibiting actin-activated myosin ATPase activity. Sparsely bound Rng2CHD induced cooperative conformational changes in actin filaments, and those actin filaments displayed a reduced affinity for the motor domain of myosin II carrying ADP, demonstrating that this

78 is a novel mode of regulation of actomyosin II motility.

79

Results

Rng2CHD strongly inhibits sliding of actin filaments on myosin II *in vitro*

To examine if Rng2 stimulates or inhibits actomyosin motility, we performed *in vitro* motility assays in which actin filaments move on a glass surface coated with myosin II (Kron and Spudich, 1986). We examined two types of myosin II, skeletal muscle myosin II and non-muscle myosin II derived from *Dictyostelium discoideum*. The movement of actin filaments was significantly inhibited by Rng2CHD on both types of myosin II (Figure 1). However, the apparent mode of inhibition was different between the two systems. On surfaces coated with full-length *Dictyostelium* myosin II, sliding velocity in the presence of 1 mM ATP was not significantly slowed by 100 - 500 nM Rng2CHD, but a large fraction of actin filaments dissociated from the myosin-coated surface in the presence of 1 μM Rng2CHD (Figure 1B and Video 1). Trajectory analyses also showed that actin filaments moving on *Dictyostelium* myosin II in the presence of Rng2CHD tended to slide sideways (Figure 1C), a phenomenon typically observed in standard *in vitro* motility assays when the surface density of myosin motor is too low.

On surfaces coated with heavy meromyosin (HMM) of rabbit skeletal muscle myosin II, in contrast, actomyosin motility in the presence of 1 mM ATP was significantly slowed in the presence of low concentrations of Rng2CHD. Movements were completely stalled, and all the filaments were virtually immobilized to the surface in the presence of 200 nM Rng2CHD (Figure 1A and Video 2). Trajectory analyses showed that under all the inhibition conditions tested using muscle HMM, the front end of the actin filament was followed by the remainder of the filament (Figure 1C). Buckling of the filaments, indicative of local inhibition of movement, was rarely observed. This indicates that movement is more or less uniformly inhibited along the entire length of the filaments on muscle HMM surfaces. Movements of actin filaments on surfaces deposited with filaments of muscle myosin II were similarly inhibited by Rng2CHD, indicating that the inhibition is not related to the mode of immobilization of myosin motors (Video 3).

The two myosin IIs differ not only in their response to Rng2CHD, but also in their sliding velocity in the absence of Rng2CHD. The latter difference can be primarily attributed to a difference in the lifetime of the force-generating A•M•ADP complex (Toyoshima et al., 1990; Uyeda et al., 1990). Indeed, previous kinetic measurements demonstrated that the dissociation of *Dictyostelium* myosin II motor carrying ADP from actin is about 5-fold slower and ATP-induced dissociation of actin-myosin motor complexes is 10-fold slower than muscle myosin II (Ritchie et al., 1993). Thus, we examined the effects of extending the lifetime of the force-generating complex of actin and muscle HMM carrying ADP (Figure 1B). In the presence of 0.2 mM ATP and 1 mM ADP, the sliding velocity by muscle HMM in the absence of Rng2CHD was slowed to 0.27 μm/s, which was expected, but was further slowed only by an additional 37% by 100 nM Rng2CHD, in contrast to 99% inhibition by the same concentration of Rng2CHD in the presence of 1 mM ATP. Similar results

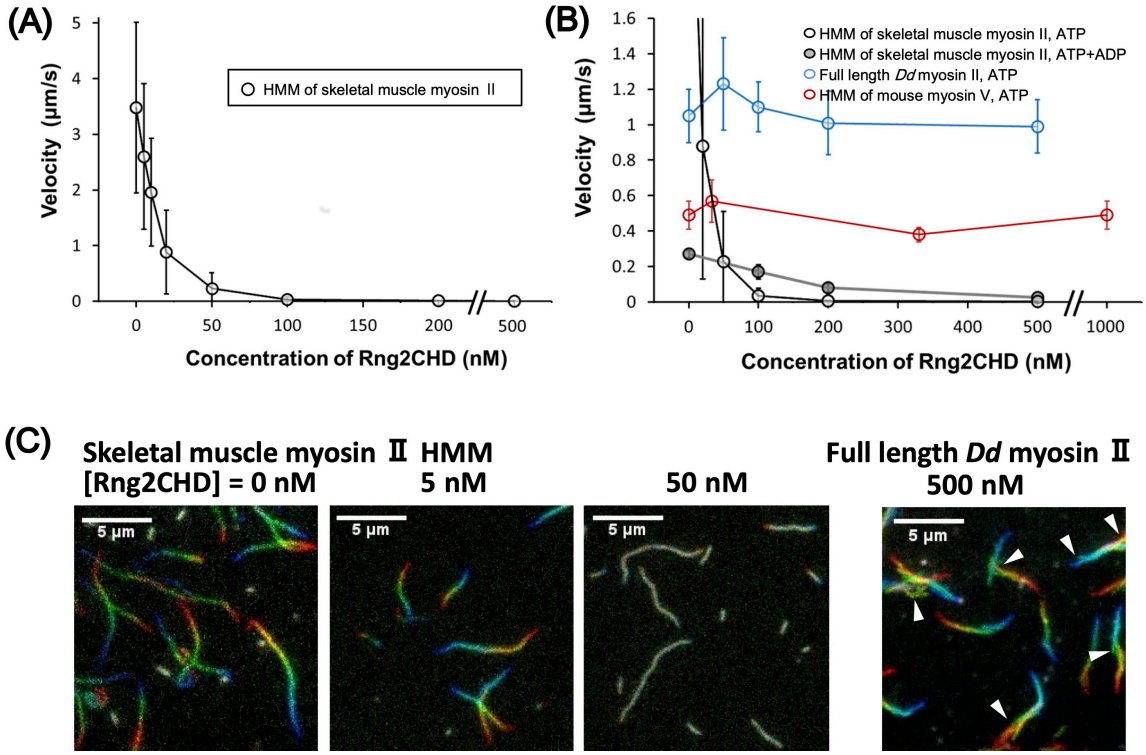

Figure 1. Rng2CHD strongly inhibits movement of actin filaments on myosin II, but not on myosin V.

(A) Movement velocity of actin filaments on muscle myosin II HMM in the presence of various concentrations of Rng2CHD. **(B)** Velocity of actin filaments on surfaces coated with muscle HMM, full length *Dictyostelium* myosin II and myosin V HMM in the presence of various concentrations of Rng2CHD. Open black circles show speeds of actin filaments by muscle HMM in the presence of 1 mM ATP, and black circles filled with gray in the presence of 0.2 mM ATP and 1 mM ADP. Open blue circles show speeds by *Dictyostelium* myosin II in the presence of 1 mM ATP, and red open circles show speeds by myosin V in the presence of 2 mM ATP. A total of randomly chosen 100-110 filaments, excluding very short filaments (<1.5 μm), were analyzed for each condition. Data are expressed as the mean ± SD. For other methods of velocity analyses, see Figure Supplement 1. The movement velocity on muscle HMM in the presence 100 nM Rng2 CHD was 0.035 ± 0.043 μm/s in the presence of 1 mM ATP and 0.17 ± 0.04 μm/s in the presence of 0.2 mM ATP and 1 mM ADP, and this difference was statistically significant ($p<10^{-37}$ by Student' *t*-test). In the presence of 200 nM Rng2CHD, the two velocities were 0.0057 ± 0.0043 μm/s and 0.079 ± 0.024 μm/s, respectively ($p<10^{-21}$). Actin velocity on *Dictyostelium* myosin II-coated surfaces was 1.1 ± 0.2 μm/s in the absence of Rng2CHD and 1.2 ± 0.3 μm/s in the presence of 50 nM Rng2CHD. This difference was statistically significant ($p<10^{-13}$ by Student's *t*-test) and was reproduced in two independent experiments. For a possible explanation for this small difference, see Supplementary information

2. In the presence of 1 μM Rng2CHD, most of the actin filaments detached from the surfaces coated with *Dictyostelium* myosin II, after brief unidirectional movements (Video 1). **(C)** Trajectories of moving actin filaments on muscle myosin II HMM in the presence of 0, 5 and 50 nM Rng2CHD, and on *Dictyostelium* myosin II in the presence of 500 nM Rng2CHD. Eleven consecutive images at 0.2 s (muscle HMM) or 0.5 s (*Dictyostelium* myosin II) intervals are coded in rainbow colors from red to blue, and overlaid. Note that actin filaments moving on *Dictyostelium* myosin II in the presence of Rng2CHD often move laterally, indicating weak affinity between actin filaments and the myosin motors (white arrowheads). Because filament ends also frequently move laterally, mean actin velocities on *Dictyostelium* myosin II in the presence of Rng2CHD, which were calculated by tracking filament ends, were overestimated.

were obtained in the presence of 200 nM Rng2CHD. Consequently, in the presence of 100 nM or 200 nM Rng2CHD, filaments moved faster in the presence of 0.2 mM ATP and 1 mM ADP than in the presence of 1 mM ATP (Video 4). Thus, extension of the A•M•ADP complex of muscle HMM partially mimicked the property of *Dictyostelium* myosin II in terms of sensitivity to Rng2CHD.

We also performed *in vitro* motility assays in which actin filaments moved on recombinant myosin V HMM that was expressed in insect cells. In striking contrast to myosin II, up to 1 μM Rng2CHD did not inhibit the sliding of actin filaments on myosin V HMM (Figure 1B and Video 5).

Rng2CHD on actin filaments inhibits actomyosin II movement on muscle HMM *in vitro* even when binding is sparse

To characterize the inhibition of motility by Rng2CHD, we decided to use fragments of muscle myosin II in the following experiments since the movement by muscle myosin II was most strongly inhibited by Rng2CHD. First, we estimated the binding ratio, or molar binding density, of Rng2CHD to actin protomers when the movement of actin filaments was potently inhibited on muscle HMM. The concentrations of Rng2CHD that caused 50%, 75% and 95% reduction of movement speed, as estimated from the velocity curve, were 12 nM, 21 nM and 64 nM, respectively (Figure 1A). In parallel, we performed co-sedimentation assays of actin filaments with Rng2CHD, and the dissociation constant (K_d) between Rng2CHD and actin protomers was calculated (Figure 2A, 2B). K_d was determined to be 0.92 μM by the following fitting function: $[Rng2CHD_{bound}] = [Actin_{total}][Rng2CHD_{free}]/([Rng2CHD_{free}] + K_d)$ (Eq. 1 in Materials and Methods).

During *in vitro* motility assays, in which the concentration of actin protomers is much lower than that of Rng2CHD, it is difficult to estimate [$Actin_{total}$], but the following approximation holds: $[Rng2CHD_{bound}]/[Actin_{free}] \cong [Rng2CHD_{total}]/K_d$ (Eq. 3 in Materials and Methods). Using

this approximation, the binding ratio of Rng2CHD to actin protomers that caused 50%, 75% and 95% reduction of actomyosin II movement speed on muscle HMM was estimated to be 1.3%, 2.2% and 6.7%, respectively (Table 1). In other words, Rng2CHD was sparsely bound to actin filaments when the speed was reduced to half, and at the Rng2CHD concentration of 100 nM, when the mean sliding velocity was reduced to 1% of the control, the binding ratio was 11%.

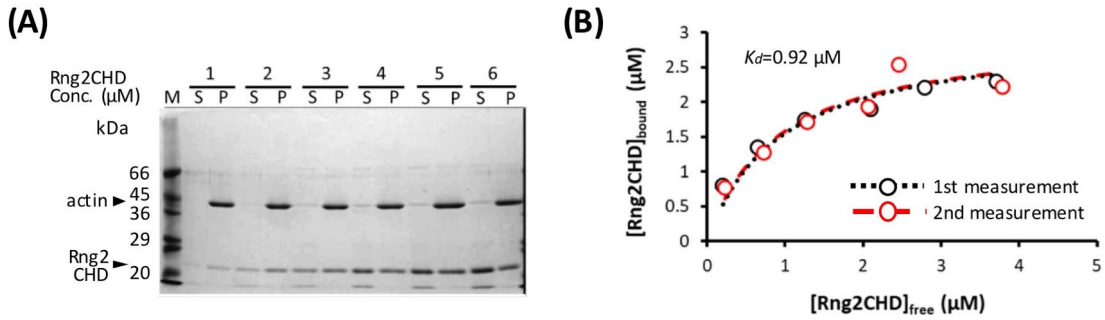

Figure 2. Measurement of K_d between actin filaments and Rng2CHD.
(A) Co-sedimentation assay of Rng2CHD with 3 μM of actin filaments. **(B)** The concentration of bound Rng2CHD was plotted against the concentration of the free fraction and fitted with the following equation: $[Rng2CHD_{bound}] = [Actin_{total}]\,[Rng2CHD_{free}] / ([Rng2CHD_{free}+K_d])$. K_d between Rng2CHD and actin protomers was calculated as an average value of the two trials.

Table 1. Estimated binding ratio of Rng2CHD and GFP-Rng2CHD to actin filaments.

Inhibition rate of movement	50%	75%	80%	90%	95%
$[Rng2CHD_{bound}]/[Actin_{total}]$	1.3%	2.2%	3.0%	4.5%	6.7%
$[GFP-Rng2CHD_{bound}]/[Actin_{total}]$	nd	nd	9.7%	21%	nd

The estimated binding ratio of Rng2CHD and GFP-Rng2CHD to actin protomers that caused various degrees of movement inhibition on muscle myosin II HMM. These values were estimated based on the following approximation: $[Rng2CHD_{total}]/K_d \cong [Rng2CHD_{bound}]/[Actin_{free}]$ for Rng2CHD, and from fluorescence intensities for GFP-Rng2CHD (Figure 3). nd: not determined.

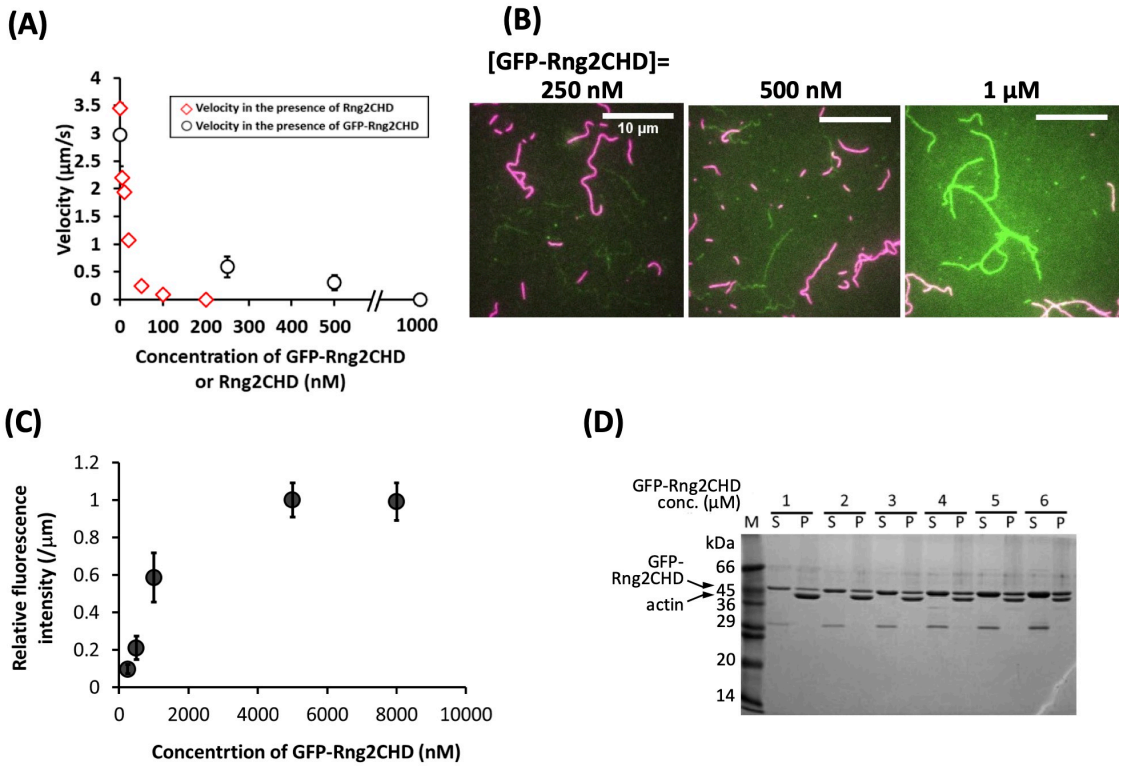

Figure 3. Sparsely bound GFP-Rng2CHD on actin filaments inhibits their movement on muscle myosin II HMM.

(A) Movement velocity of actin filaments on muscle myosin II HMM-coated glass surfaces in the presence of various concentration of GFP-Rng2CHD (black plots). Ten smoothly moving filaments were chosen for each condition, and approximately 10 consecutive measurements were made for each filament. Data are expressed as the mean ± SD. Movement velocity in the presence of Rng2CHD is also shown for the reference (red plots). **(B)** Fluorescence micrographs of GFP-Rng2CHD bound to actin filaments. Actin filaments stabilized by non-fluorescent phalloidin and those labeled with rhodamine phalloidin were present at a 1:1 molar ratio. Green: GFP fluorescence. Red: rhodamine fluorescence. Non-fluorescent phalloidin-stabilized actin filaments were used to quantify the intensity of GFP fluorescence, since there was a low level of leakage of rhodamine fluorescence in the GFP channel, which could disturb the measurement of GFP fluorescence. Rhodamine-phalloidin–labeled actin filaments were used to measure sliding speed. Bars: 10 μm. **(C)** Fluorescence intensity of GFP-Rng2CHD on non-fluorescent phalloidin-stabilized actin filaments. Fluorescence intensity along five filaments was measured for five frames. Data are expressed as the mean ± SD of 25 measurements. **(D)** Cosedimentation of GFP-Rng2CHD with 3 μM of actin filaments. Similar molar amounts of actin and GFP-Rng2CHD were recovered in the pellet fractions when [GFP-Rng2CHD] was 5 and 6 μM. The GFP-Rng2CHD preparation was contaminated by a bacterial ~30 kDa protein.

To directly confirm that sparsely bound Rng2CHD potently inhibits actomyosin movements on muscle HMM, we prepared Rng2CHD fused with GFP to its N-terminus via a 16-residue linker (GFP-Rng2CHD), and determined the binding ratio of GFP-Rng2CHD to actin protomers from the fluorescence intensity of GFP. GFP-Rng2CHD strongly inhibited actin filament movement on muscle HMM in a manner similar to Rng2CHD (Figure 3A). We then measured the fluorescence intensity of bound GFP-Rng2CHD per unit length of actin filaments. Fluorescence intensity increased depending on the GFP-Rng2CHD concentration in the buffer, and was saturated in the presence of 5 μM GFP-Rng2CHD (Figure 3B, 3C). The co-sedimentation assay showed that one molecule of GFP-Rng2CHD binds to one molecule of an actin protomer in the presence of 5 μM GFP-Rng2CHD (Figure 3D). Therefore, we regarded this saturated fluorescence intensity as a one-to-one binding state, and used it as the reference to calculate how much GFP-Rng2CHD binds to actin protomers when movements were inhibited in the presence of lower concentrations of GFP-Rng2CHD. This fluorescence-based direct quantification also demonstrated that sparsely bound GFP-Rng2CHD strongly inhibits actin movements on muscle HMM (Table 1), although based on these directly measured binding ratios of GFP-Rng2CHD to actin protomers, a higher binding ratio was needed to obtain the same degree of motility inhibition than that estimated from K_d using unlabeled Rng2CHD. Similarly higher binding ratios needed to obtain the same degree of motility inhibition were obtained when the binding ratio of GFP-Rng2CHD was estimated from K_d that was derived from the cosedimentation experiments (Supplementary Information 1).

Rng2CHD cooperatively changes the structure of actin filaments, accompanying supertwisting and local kinks or structural distortions

Based on the very low binding ratio of Rng2CHD required to inhibit movement of actin filaments on muscle myosin II, we inferred that sparsely bound Rng2CHD somehow induces global structural changes in actin filaments and inhibits actomyosin II movement. To examine whether sparsely bound Rng2CHD actually changes the structure of actin filaments, we observed actin filaments in the presence of Rng2CHD using negative stain electron microscopy and high speed atomic force microscopy (HS-AFM).

For HS-AFM observations, actin filaments were loosely immobilized on a positively charged lipid bilayer, the condition which we previously used to detect cofilin-induced supertwisting of actin filaments (Ngo et al., 2015). Periodic patterns representing half helices of the double-helical structures were clearly observed, in which the tallest parts in each half helix, or the crossover points, are shown in a brighter color (Figure 4A). In the presence of 0.59 μM actin and 20 nM Rng2CHD, no bound Rng2CHD molecules were detected, although the binding ratio estimated from K_d was 1.3%. When the concentration of Rng2CHD was increased to 0.25 μM, which corresponds to the estimated binding ratio of 15%, we were able to detect sparse and transient binding events (Figure

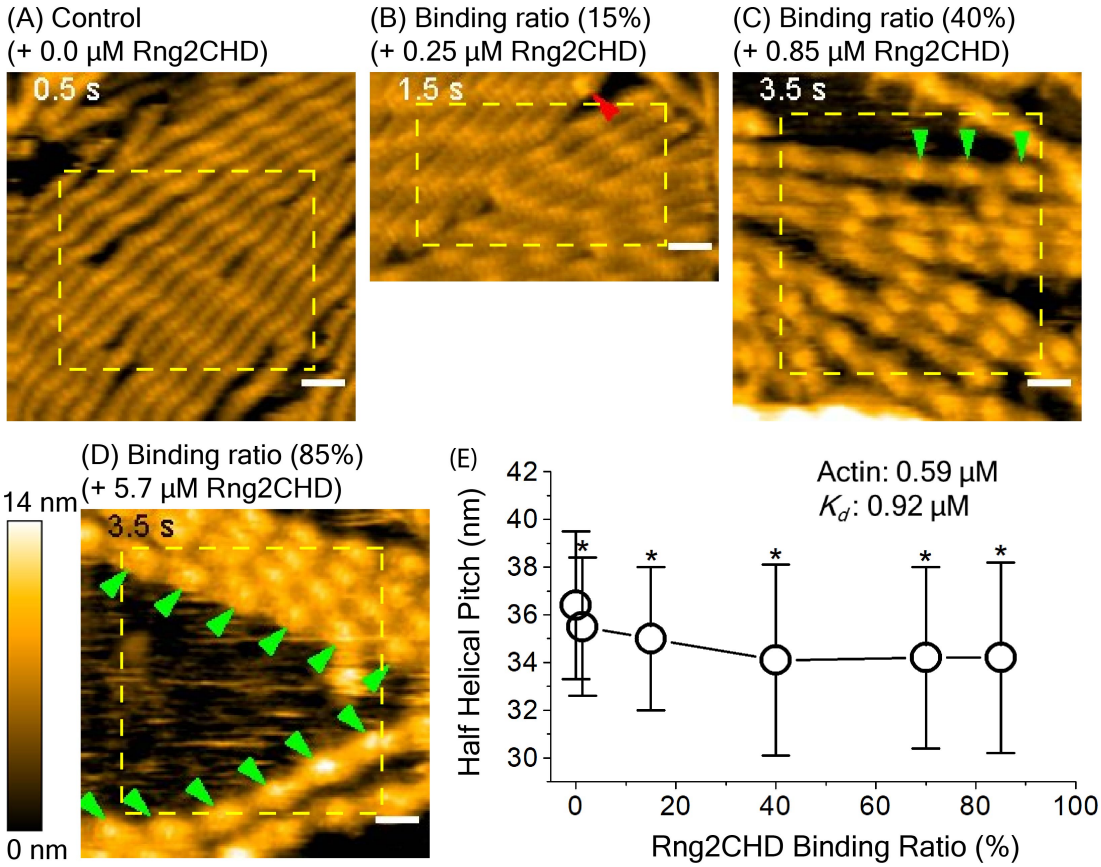

Figure 4. HS-AFM imaging and analysis of half helical pitch (HHP) of actin filaments at different Rng2CHD binding ratios.

Actin filaments were premixed with Rng2CHD at different concentrations in a tube for 10 min at RT to achieve equilibrium binding. These protein mixtures (68 µl) were introduced into an observation chamber for HS-AFM imaging, and actin filaments with and without bound Rng2CHD were gently immobilized onto positively-charged lipid bilayer formed on mica. In all experiments, the concentration of actin filaments was fixed at 0.59 µM while the concentrations of Rng2CHD were varied at 0, 0.020, 0.25, 0.85, 2.6, and 5.7 µM. Typical images of actin filaments at different Rng2CHD binding ratios are shown in **A-D**. Red and green arrowheads denote isolated and series of Rng2CHD clusters, respectively. Note that only selected series of the Rng2CHD clusters are marked. Bars: 25 nm. Using those images, half helical pitches (HHPs) were estimated by measuring the distances between the peaks of two neighboring two half helices. Half helices in the yellow rectangles were subjected to the HHP measurements, regardless of the presence or absence of Rng2CHD clusters. The Rng2CHD binding ratio was estimated by using the K_d value of 0.92 µM. The correlation between Rng2CHD binding ratio and HHP of actin filaments is shown in **E**. The values are mean HHP ± SD. Note that the position of the peak (highest point of the actin protomer that is closest to the crossover point) does not necessarily coincide with the crossover point of two

helices that connect the centers of the mass of actin protomers in each protofilament, and there can be up to 5.5/2 nm error between the two positions. This error would not affect the mean of HHPs, since they would be averaged out when multiple HHPs are measured consecutively along actin filaments, but would contribute to the larger SD values (Ngo et al., 2015). The statistical differences of the mean HHP of control actin filaments (0 μM Rng2CHD) and that at different Rng2CHD binding ratios (*, $p \leqq 0.001$, two independent populations *t*-test) were calculated. **Related to Video 6 and Table Supplement 1**.

4B and Video 6). In the image shown in Figure 4B, there are approximately 57 half helices, or approximately 740 actin protomers, implying that there must be 110 bound Rng2CHD molecules in this image. However, there is only one Rng2CHD-derived bright spot in this image. Those bright spots appear and disappear transiently, but the number of Rng2CHD spots that could be detected simultaneously in this imaging field did not exceed two during the 14.5 s of observation (Video 6). Regarding this apparently large discrepancy, it is notable that all the Rng2CHD-derived bright spots appeared at the crossover points of the double helix (Video 6). Moreover, all the Rng2CHD-derived bright spots were as large as or larger than actin protomers (42 kDa) and some bright spots obviously consisted of two smaller bright spots. We thus speculate that what we imaged were clusters of two or more Rng2CHD molecules bound near the crossover points, and individual bound Rng2CHD molecules and the clusters that bound along the filament sides were not efficiently imaged due to the small size (21 kDa).

In the presence of 0.85 and 2.6 μM Rng2CHD, which correspond to the estimated binding densities of 40% and 70%, respectively, progressively larger fraction of crossover points became brighter, while other crossover points remained unchanged (Figure 4C), again suggesting the propensity of Rng2CHD to form clusters. In the presence of 5.7 μM Rng2CHD, which corresponds to the estimated binding ratio of 85%, most of the crossover points were brighter (Figure 4D), implying a nearly saturated binding. We then measured half helical pitches (HHP) of actin filaments by measuring the distances between the crossover points under equilibrium binding conditions, and found that Rng2CHD induced shortening of HHP, or supertwisting (Figure 4E). Strikingly, the supertwisting conformational changes nearly saturated at 0.85 μM Rng2CHD, when the estimated binding ratio was 40%. These results clearly demonstrate that sparsely bound Rng2CHD induces cooperative conformational changes to actin filaments. Another notable feature of actin filaments in the presence of Rng2CHD is the transient local untwisting of the helix to result in two separate protofilaments (Figure Supplement 3 and Video 7).

We also employed frequency modulation atomic force microscopy (FM-AFM) to observe the structural changes on actin filaments induced by Rng2CHD (Figure Supplement 4A). FM-AFM

has emerged as a powerful tool to provide nanostructural information for various surfaces/interfaces and biological samples in liquid environments with unprecedented spatial resolution (Giessibl, 2003; Ido et al., 2013). FM-AFM observation confirmed Rng2CHD-induced decrease of HHP (Figure Supplement 4B).

Negative staining and electron microscopic observation of actin filaments in the absence of Rng2CHD showed long and straight filaments (Figure 5A), and the higher magnification images were consistent with previously known helical structures (Figure 5E). However, when the actin filaments were allowed to interact with Rng2CHD in solution, then deposited onto carbon-coated grids and negatively stained (Figure 5B-5D), the appearance of filaments became irregular and more filaments became bundled. At higher concentrations (200 nM – 1 μM) of Rng2CHD, the filaments were frequently distorted, kinked, or even fragmented. Even those filaments that appeared straight often showed irregular helical structures at high magnifications (Figure 5F-5H): the two actin protofilaments appeared to be separated in some portions of the filaments, so that a dark straight line was observed in between two parallel protofilaments (indicated by yellow brackets). The observed separation of the protofilaments presumably correspond to the parallel protofilaments observed by HS-AFM (Figure Supplement 3), indicating that they are not artifacts of HS-AFM or negative staining. Such Rng2CHD-induced local untwisting conformational changes appear at odds with the Rng2CHD-induced supertwisting observed by HS-AFM. Since the local untwisting was frequently observed in the medium concentration range of Rng2CHD, we speculate that the local untwisting is a compensatory conformational change that is induced by Rng2CHD-induced local supertwisting and facilitated by Rng2CHD-induced weakening of interactions between the protofilaments.

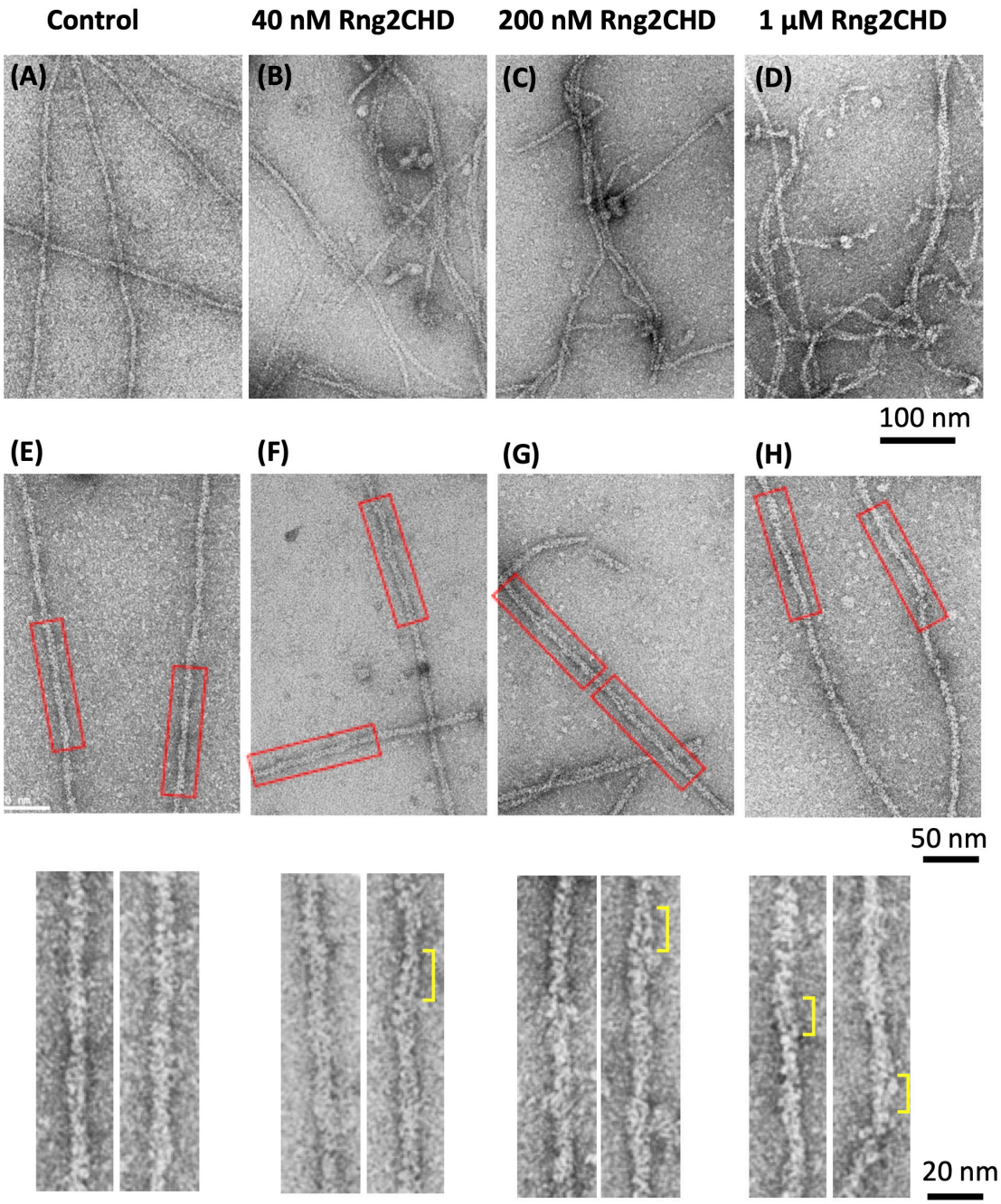

Figure 5. Rng2CHD deforms the helical structures of actin filaments.

Electron micrographs of negatively stained actin filaments in the absence **(A, E)** and presence of 40 nM **(B, F)**, 200 nM **(C, G)** and 1 µM **(D, H)** Rng2CHD. In the presence of Rng2CHD, the filaments were often bundled and kinked. In the presence of high concentrations of Rng2CHD, the filaments were highly deformed and showed discontinuities (**C** and **D**), which can be explained by altered interactions between neighboring actin protomers. **E**, **F**, **G** and **H** are higher magnifications of the

331 straight portions of the filaments under each condition, and the boxed regions are further magnified
332 in the bottom row. In some parts, the two actin protofilaments look separated (yellow brackets),
333 suggesting that Rng2CHD somehow reduces, or at least changes, the interaction between the two
334 protofilaments at sub-stoichiometric binding ratios. In the absence of Rng2CHD, such irregular
335 filament structures were not observed **(A, E)**.
336
337
338 **Steady state actin-activated muscle S1 ATPase is only weakly inhibited by Rng2CHD**
339 To gain insight into the mechanism by which structural changes of actin filaments induced by
340 Rng2CHD inhibit motility by muscle myosin II, we investigated the effects of Rng2CHD on actin-
341 activated ATPase activity of muscle myosin II subfragment-1 (S1). Actin-activated S1 ATPase was
342 moderately inhibited (approximately 50%) by the highest concentration of Rng2CHD tested (5 μM;
343 Figure 6). In the presence of 0.33 μM and 0.82 μM Rng2CHD and 24 μM of actin filaments, the
344 actin-activated S1 ATPase activity was not inhibited in a statistically significant manner. Under those
345 conditions, the binding ratios of Rng2CHD to actin were calculated as 1.3% and 3.7% (Eq. 2 in
346 Materials and Methods), which caused a 50% and 82% reduction in the speed of actin movement,
347 respectively, by muscle HMM (Figure 1A and Table 1). In the presence of 1.9 μM Rng2CHD, S1
348 ATPase was inhibited by 29%, which was statistically significant ($p<0.03$). In this condition, the
349 binding ratio was calculated as 7.6%, which inhibited 96% of sliding speed. Thus, the inhibition of
350 actin-activated S1 ATPase activity was much weaker and disproportional to the inhibition of
351 movement (Figure 6). This indicates that Rng2CHD-induced strong inhibition and stalled actin
352 movements on muscle HMM do not necessarily accompany inhibition of the ATPase cycle.
353

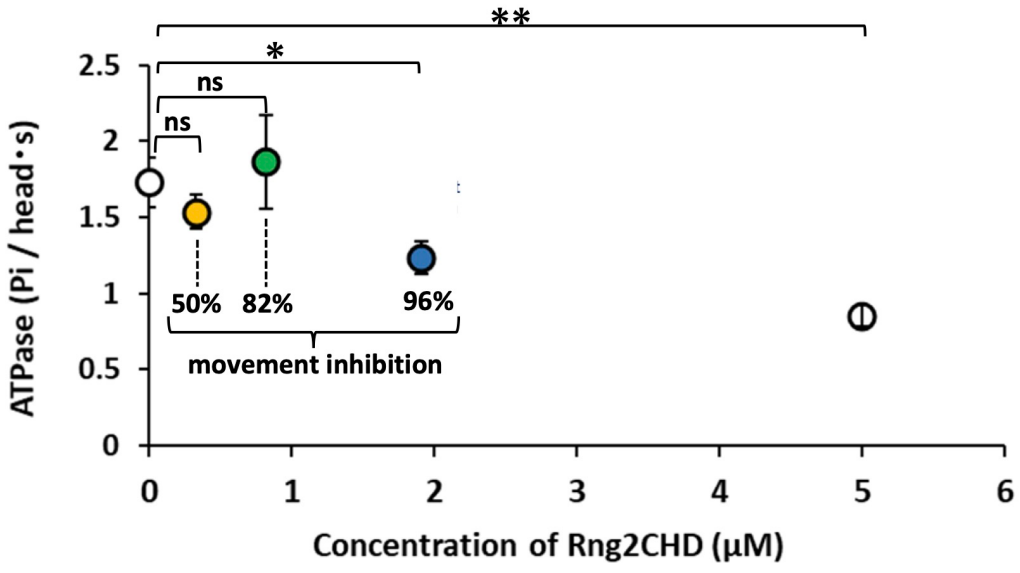

Figure 6. Actin-activated muscle S1 ATPase in the presence of Rng2CHD.
The orange (0.33 μM Rng2CHD), green (0.82 μM Rng2CHD) and blue (1.9 μM Rng2CHD) plots were measured in the presence of Rng2CHD concentrations that were expected to bind to actin protomers at binding ratios which caused a 50%, 82% and 96% reduction of actomyosin movement speed on muscle HMM, respectively during *in vitro* motility assays. Note that the concentration of Rng2CHD to achieve the same binding ratio is very different between this ATPase experiment and the motility assays because the concentration of actin is very different between the two experiments. Data are expressed as the mean ± SD of three independent experiments. "ns" indicates that the differences are not statistically significant; "*" and "**" indicate statistically significant differences with a p value < 0.03 and < 0.002, respectively, according to a Student's t-test.

Rng2CHD inhibits the steady-state binding of muscle S1 to actin filaments in the presence of ADP, but not in the presence of ATP

We examined the possibility that Rng2CHD might affect the affinity between actin filaments and myosin motor when it inhibits motility by muscle HMM. First, we performed a co-sedimentation assay of actin filaments and muscle S1, and found that Rng2CHD did not significantly inhibit steady-state binding of S1 to actin filaments in the presence of ATP (Figure 7A, 7C). However, Rng2CHD weakly but statistically significantly inhibited the binding of S1•ADP to actin filaments in the presence of ADP in the buffer (Figure 7B, 7C).

A co-sedimentation assay using muscle myosin II filaments showed that Rng2CHD only weakly bound to myosin II under the conditions employed in the *in vitro* motility assays (Figure Supplement 5).

We also employed HS-AFM to directly observe transient binding of muscle S1 molecules to actin filaments in the presence of ATP. At a scan speed of 0.5 s per field of view, transient binding of S1 to actin filaments was rarely observed in the presence of 500 μM ATP alone, but was frequently observed in the presence of 50 μM ATP and 1 mM ADP. S1 molecules were easily identified based on their size and shape, whereas individual bound Rng2CHD molecules were not visualized as described earlier. We analyzed images scanned between 1 and 2 min after the addition of S1, and visually counted the number of transient binding events of S1 molecules (Figure 8A). The binding dwell time of S1 molecules on the top of the filament was shorter than those bound along the sides of the filaments. Therefore, we separately counted the S1 molecules bound on the top and along the sides of the filaments. The number of S1 molecules that transiently bound to actin filaments was significantly lower when 12 nM Rng2CHD, the concentration that caused 50% inhibition of motility on muscle HMM, was added before the addition of S1 (Figure 8B, 8C). It was thus directly confirmed that sparsely bound Rng2CHD affected the binding of S1 to actin filaments

390 in the presence of ATP and ADP.

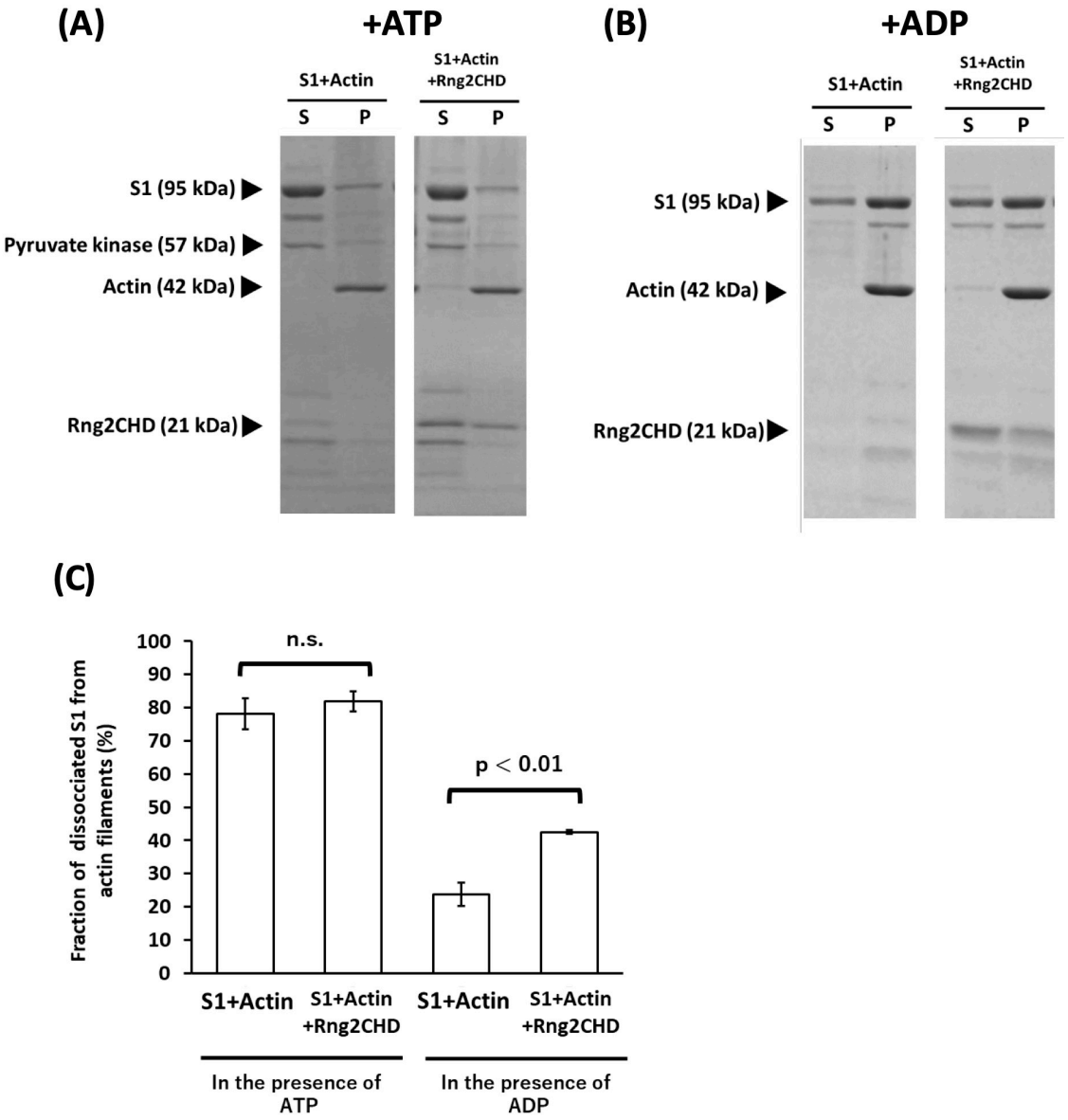

391

392 **Figure 7. Rng2CHD inhibits the steady-state binding of S1 to actin filaments in the presence of**
393 **ADP, but not in the presence of ATP.**
394 **(A, B)** Co-sedimentation assay of S1 and actin filaments in the presence of Rng2CHD and 2 mM
395 ATP (A) or 2 mM ADP (B). **(C)** Fraction of S1 dissociated from actin filaments was compared with
396 and without Rng2CHD. Rng2CHD significantly increased the fraction of dissociated S1 from actin
397 filaments in the presence of ADP (Student's *t*-test, $p<0.01$), but not in the presence of ATP. Data are
398 expressed as the mean ± SD of three independent experiments.
399
400

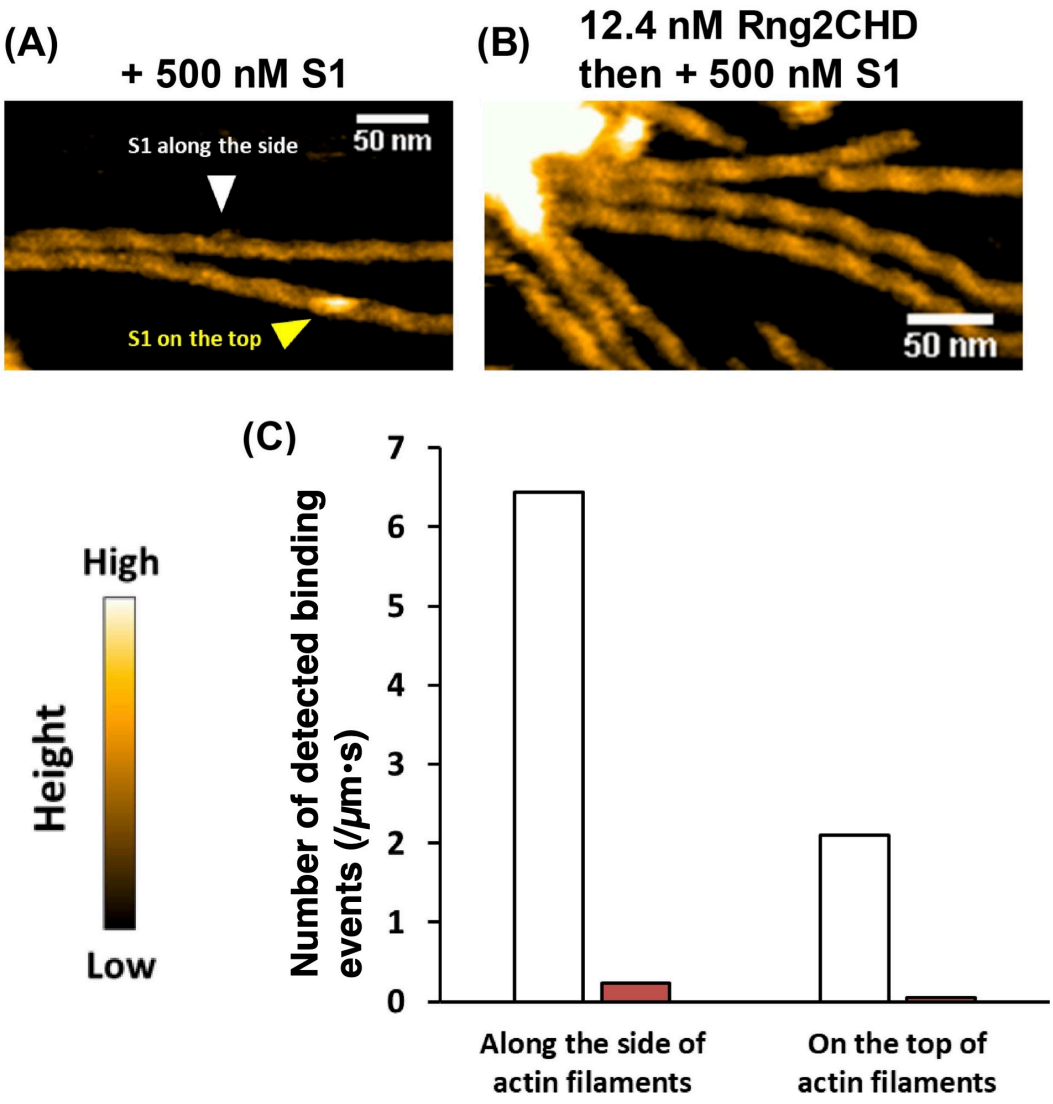

Figure 8. Rng2CHD significantly decreases the number of S1 molecules bound along actin filaments in the presence of ATP and ADP.

(A, B) HS-AFM images of actin filaments interacting with S1 in the presence of 50 μM ATP and 1 mM ADP. The images were scanned at about 2 min after the addition of 500 nM S1. S1 molecules that bound on the top and along the side of the filaments are indicated by yellow and white arrowheads, respectively. In **(A)**, 500 nM S1 was added to actin filaments. In **(B)**, in contrast, actin filaments were preincubated with 12 nM Rng2CHD for 15 min, then 500 nM S1 was added. **(C)** Number of observed S1 binding events on the top or along the sides of the filaments in the presence of 50 μM ATP and 1 mM ADP. The values were normalized by the total length of the measured filaments and time. White bars: 500 nM S1 was added to actin filaments. Red bars: Actin filaments were preincubated with Rng2CHD, and then 500 nM S1 was added. The number of bound S1 molecules was counted in the images scanned between 1 and 2 min after the addition of S1.

The result that transient binding of S1 molecules to actin filaments was hardly observed in the presence of 500 μM ATP alone suggests that, in the presence of 50 μM ATP and 1 mM ADP, HS-AFM presumably detected S1•ADP bound to actin filaments before the low concentration of ATP in the presence of excess ADP slowly disrupted the binding. The decrease in the number of detected S1 molecules caused by Rng2CHD can be interpreted in the following two ways: (1) the number of transient binding events of S1 decreased, or (2) the duration of each binding event was shortened. Hypothesis (1) predicts that actin-activated S1 ATPase is also very strongly inhibited by Rng2CHD, which was not the case. We thus concluded that the unstable binding of S1•ADP to actin filaments caused by Rng2CHD shortened the duration of transient binding of S1•ADP to actin filaments, and decreased the efficiency of detection of transient binding by HS-AFM.

Rng2CHD decreases the fluorescence of HMM-GFP along actin filaments in the presence of ATP

We previously reported that when HMM of *Dictyostelium* myosin II fused with GFP was allowed to interact with actin filaments in the presence of a very low concentration of ATP, HMM-GFP formed clusters along actin filaments (Tokuraku et al., 2009; Hirakawa et al., 2017). This was interpreted to represent local polymorphism of actin filaments, such that some segments of the filaments have a higher affinity for HMM than other parts of the filament, and HMM-GFP preferentially repeats transient binding to those segments. In the presence of a high concentration of ATP, no fluorescent clusters were observed, and in the absence of ATP, HMM-GFP uniformly bound along the entire filaments (Tokuraku et al., 2009).

We speculated that, in order for the detectable fluorescent clusters to form, HMM needs to bind to actin filaments repetitively and transiently, although the dwell time of each binding event must be long enough to allow visualization. Based on this hypothesis, we employed fluorescence microscopy to observe how Rng2CHD affected the formation of *Dictyostelium* HMM-GFP clusters along actin filaments in the presence of a very low concentration of ATP. Numerous fluorescent spots, each representing an HMM-GFP cluster, were observed along actin filaments in the presence of 0.5 μM ATP and in the absence of Rng2CHD. In the presence of 1 nM Rng2CHD, the number and fluorescence intensity of fluorescent spots were significantly reduced, and fluorescent spots were apparently absent in the presence of 10 nM Rng2CHD (Figure 9A, 9C). In contrast, Rng2CHD did not affect the binding of HMM-GFP to actin filaments in the nucleotide-free state (Figure 9B, 9C).

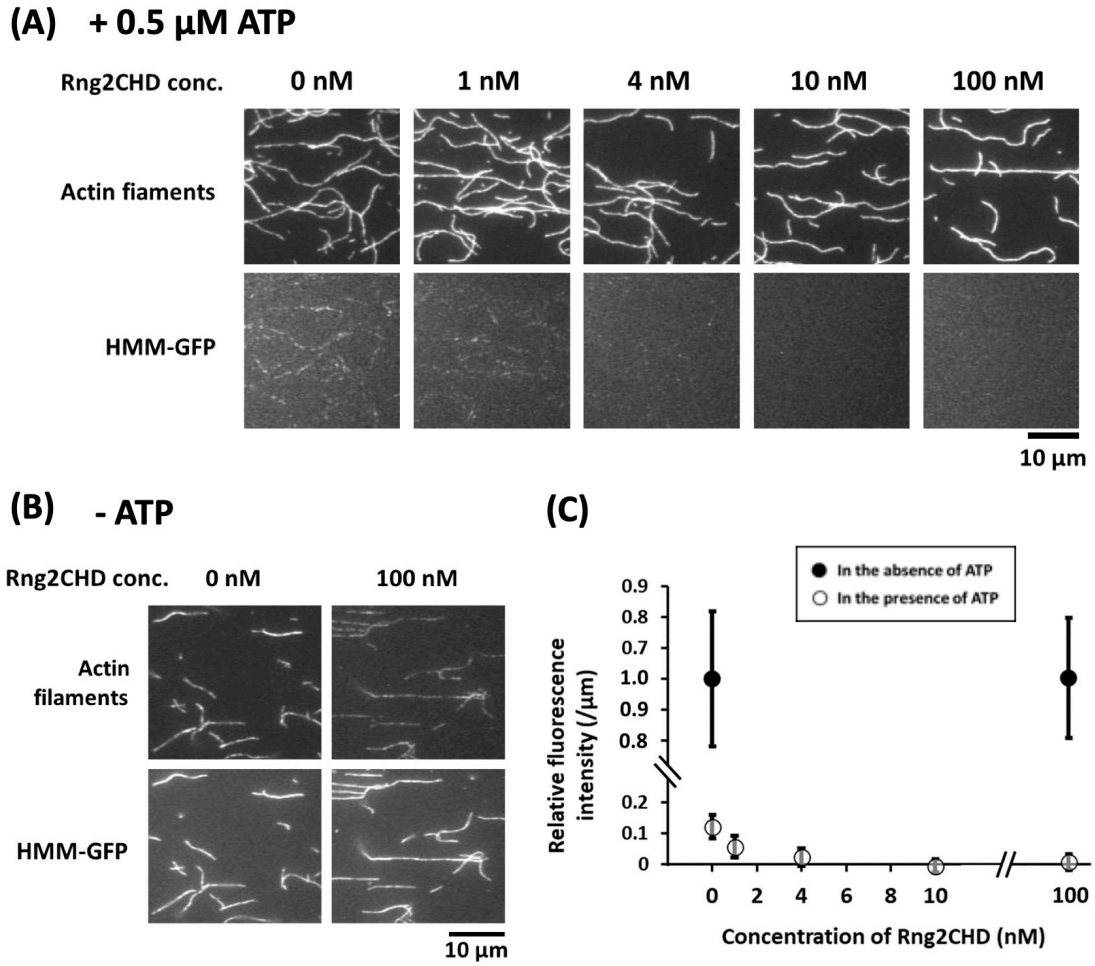

Figure 9. Rng2CHD decreases the fluorescence of HMM-GFP along actin filaments in the presence of ATP.

Fluorescence micrographs of actin filaments labeled lightly with Alexa647 phalloidin and *Dictyostelium* HMM-GFP in the presence of 0.5 µM ATP **(A)** and in the nucleotide-free state **(B)**. In each panel, the top row shows the fluorescence of Alexa647, and the bottom row shows that of GFP. Fluorescence intensity of GFP was measured along each actin filament and divided by the length of the filament, and mean and SD of the resultant values were calculated for each condition (N=20). These normalized GFP fluorescence intensities were further normalized against the value in the absence of ATP and Rng2CHD to obtain relative fluorescence intensity (**C**). Filled circles show the data in the absence of ATP and the open circles show the data in the presence of 0.5 µM ATP. The binding ratio of Rng2CHD along the actin filaments, estimated from K_d, are 0.1, 0.4, 1.1 and 9.8% for the Rng2CHD concentrations of 1.0, 4.0, 10 and 100 nM, respectively.

Discussion

Structural changes of actin filaments induced by sparsely bound Rng2CHD inhibit actomyosin II movement

Rng2CHD, the actin-binding domain of Rng2, strongly inhibited actomyosin II motility, and particularly potently on skeletal muscle myosin II. Inhibition occurred along the entire length of the filament on muscle HMM, when actin filaments were only sparsely decorated by Rng2CHD or GFP-Rng2CHD (Figure 1A, 3A, Video 2, and Table 1). Since binding of Rng2CHD or GFP-Rng2CHD was sparse, the inhibition of motility could not be due to steric hindrance or direct competition for a binding site on actin molecules. We thus inferred that sparsely bound Rng2CHD induced some cooperative structural changes in actin filaments, and these inhibited the productive interaction between actin filaments and myosin II. Previous studies advocated that structural changes of actin filaments modulate affinities for various ABPs (Ngo et al., 2016; Shibata et al., 2016; Harris et al., 2020). For example, cofilin cooperatively binds to actin filaments to form clusters along the filaments, reducing the helical pitch of filaments in the cluster by 25% (McGough et al., 1997). Notably, this structural change was propagated to the neighboring cofilin-unbound bare region (Galkin et al., 2001; Ngo et al., 2015), and this was accompanied by decreased affinity for muscle S1 in the presence of ATP (Ngo et al., 2016). In this study, HS-AFM observation showed that Rng2CHD cooperatively changed the structure of actin filaments accompanying supertwisting even when Rng2CHD was only sparsely bound to actin filaments (Figure 4E). Discontinuities and kinks of the actin filaments, as well as the dark straight lines between the two protofilaments observed by electron microscopy (Figure 5), suggest that the interaction between actin protomers were altered by Rng2CHD at sub-stoichiometric binding densities. Although the extent of supertwisting by Rng2CHD (~5%) was much smaller than that caused by cofilin, it is notable that Rng2CHD and cofilin share two properties, namely supertwisting of the actin helix, and a decreased affinity for myosin II. Elucidating whether there is a causal relationship between the two properties or they are mere coincidence needs further investigations.

We consider two possible mechanisms by which sparsely bound Rng2CHD inhibits actomyosin II movements. The first mechanism proposes that one or two actin protomers in direct contact with the bound Rng2CHD molecule undergo structural changes, and those affected actin protomers bind persistently to myosin II motors even in the presence of ATP, acting as a potent break. The second mechanism assumes that a bound Rng2CHD molecule changes the structure of multiple actin protomers, and the affected actin protomers become unable to productively interact with myosin II. The first mechanism predicts that Rng2CHD should increase the amount of co-sedimented S1 in the presence of ATP, which was not the case (Figure 7A, 7C). Direct observation of actin binding of *Dictyostelium* myosin II HMM-GFP in the presence of a very low concentration of ATP also demonstrated that Rng2CHD decreased the affinity between actin filaments and myosin II

motors in a concentration-dependent manner (Figure 9A, 9C). Furthermore, buckling of the moving actin filaments on muscle HMM-coated surfaces, indicative of local inhibition of the movement, was rarely observed in the presence of various concentrations of Rng2CHD (Figure 1C). The tendency of actin filaments on *Dictyostelium* myosin II to slide sideways and to detach from the myosin-coated surface is also inconsistent with the local break hypothesis. Those reasons led us to reject the first mechanism and conclude that force generation by myosin II is inhibited in broad sections of actin filaments that are not in direct contact with Rng2CHD.

Hereafter, we resolve the inhibition process into two aspects, and discuss their respective mechanisms. The first is the mechanism by which sparsely bound Rng2CHD causes global structural changes in actin filaments. The second is the mechanism by which the structural changes of actin filaments inhibit actin motility driven by myosin II.

The mechanism by which Rng2CHD causes global structural changes in actin filaments

We now consider two hypotheses for the mechanism by which one molecule of Rng2CHD changes the structure of multiple actin protomers. The first is a cooperative structural change, in which one molecule of Rng2CHD bound to one actin protomer changes the structure of multiple neighboring actin protomers in the same filament. Such cooperative propagation of conformational changes has been reported for many ABPs. The best characterized case is the propagation of a supertwisted structure in the cofilin clusters to neighboring bare zones (Galkin et al., 2001; Ngo et al., 2015). Moreover, a single molecule of gelsolin bound to the barbed end of an actin filament changes the structure of all actin protomers in the filament (Orlova et al., 1995). Other ABPs such as myosin II (Oosawa et al., 1973; Miki et al., 1982; Prochniewicz et al., 2010), tropomyosin (Khaitlina et al., 2017), α-actinin (Singh et al., 1981) and formin (Papp et al., 2006) also cause cooperative structural changes of actin filaments even at significantly sub-stoichiometric concentrations to actin monomers. The second hypothesis is the memory effect, in which Rng2CHD molecules repeat transient binding to different actin protomers, which remain in an altered conformation for a certain period of time after dissociation of Rng2CHD. If there is a memory effect, Rng2CHD can alter the structure of entire actin filaments even when its binding ratio to actin protomers is low. We speculate that either or both of these two mechanisms, cooperative structural change and memory effect, underlie the global structural changes in actin filaments induced by sparsely bound Rng2CHD.

The mechanism by which structural changes of actin filaments inhibit actomyosin II motility

Rng2CHD inhibited steady-state binding of S1•ADP to actin filaments (Figure 7B, 7C). Consistent with this result, HS-AFM demonstrated that Rng2CHD significantly reduced the binding dwell time of muscle S1 molecules on actin filaments in the presence of 50 μM ATP and 1 mM ADP (Figure 8). Moreover, fluorescence microscopy demonstrated that Rng2CHD significantly decreased the region

along actin filaments where *Dictyostelium* HMM-GFP fluorescence was observed in the presence of 0.5 μM ATP (Figure 9A).

Based on this conclusion, we propose two possible mechanisms for inhibition of actomyosin II movement caused by Rng2CHD, in the framework of the swinging lever arm model (Huxley, 1969; Cooke et al., 1984; Tokunaga, 1991; Uyeda et al., 1996) tightly coupled with the actomyosin ATPase cycle (Lymn and Taylor, 1971). The first mechanism proposes that phosphate release from myosin II•ADP•Pi is promoted normally by actin filaments that have been structurally altered by Rng2CHD, but without the lever arm swing that normally accompany the phosphate release. Consequently, myosin II•ADP, which does not have the authentic post-power stroke structure, cannot gain the normal high affinity to actin filaments. The second mechanism assumes that although the lever arm swing occurs following phosphate release, the myosin II motor domain•ADP slips at the contact surface with actin filaments, or myosin II•ADP dissociates from actin filaments, because of the low affinity between myosin II•ADP and the structurally altered actin filaments. This would lead to a failure of myosin II•ADP to maintain the tension, generated by the swing of the lever arm, to drive the movement of the actin filaments. The two inhibition mechanisms are both derived from a defective interaction between the affected actin and myosin motor carrying ADP, and may not be mutually exclusive. The two myosin IIs used in this study, i.e., skeletal muscle myosin II and *Dictyostelium* myosin II, appeared to respond differently to Rng2CHD-affected actin filaments, but the differences can be explained, at least in part, by known quantitative differences between the two myosin IIs within the framework of this proposed mechanism of inhibition (Supplementary Information 2).

Actin movements by myosin V HMM were even more different in terms of sensitivity to Rng2CHD, in that the sliding velocity by myosin V was not appreciably affected by up to 1 μM of Rng2CHD. In line with this finding, it is worth mentioning that two actin mutations, M47A (Kubota et al., 2009) and G146V (Noguchi et al., 2012), inhibit actin movements on muscle myosin II, but not on myosin V. Further studies are needed to understand the mechanism by which myosin II and V respond qualitatively differently to inhibition by Rng2CHD and certain actin mutations.

Future studies

Further investigations are also warranted to reveal the structural aspects of the inhibition of actomyosin II movement induced by Rng2CHD, and to clarify the relationship between the structural changes of actin filaments and actomyosin II motility.

Phosphorylation of the myosin light chain (Higashi-Fujime, 1983; Sellers et al., 1985; Griffith et al., 1987) and calcium regulation via tropomyosin and troponin (Ebashi and Kodama, 1965; Ebashi and Kodama, 1966) are two widely known major regulatory mechanisms of actomyosin II movements. Additionally, it has been reported that caldesmon and calponin inhibit the

568 movement of actin filaments on smooth muscle myosin II (Shirinsky et al., 1992). Of those two
569 classic regulators of smooth muscle contraction, calponin is homologous to Rng2CHD. Moreover,
570 these ABPs are similar to Rng2CHD in that they inhibit actomyosin II movements even with sparse
571 binding to actin filaments (Shirinsky et al., 1992), although the cooperativity of motility inhibition
572 on muscle HMM is weaker than that of Rng2CHD. More information is needed to further discuss the
573 mechanistic similarities and differences among the inhibition by Rng2CHD, calponin and
574 caldesmon.
575 The physiological significance of the inhibitory effect of Rng2CHD on actomyosin II is
576 another unresolved issue. Since contraction of the CR appears to be regulated in an inhibitory
577 manner (Supplementary Information 3), it is plausible that Rng2CHD plays a role in this regulatory
578 process. Recently, Palani et al. (2021) demonstrated that Rng2CHD, or “curly” according to their
579 nomenclature, that was loosely immobilized on a lipid membrane formed rings of actin filaments *in*
580 *vitro*, suggesting that it is involved in the formation of CRs *in vivo*. However, a previous truncation
581 study showed that *S. pombe* cells expressing mutant Rng2 lacking the CHD are able to assemble and
582 contract CRs normally (Tebbs and Pollard, 2013). Molecular and cell biological studies are thus
583 needed to understand the physiological role of Rng2CHD, including possible functional redundancy
584 with α-actinin, overexpression of which significantly slows cytokinesis in mammalian cells
585 (Mukhina et al., 2007).

Materials and Methods

Protein purification

Actin was purified from rabbit skeletal muscle acetone powder (Spudich and Watt, 1971; Pardee and Spudich, 1982). HMM and S1 of muscle myosin II were prepared by digestion of rabbit skeletal muscle myosin with papain and α-chymotrypsin, respectively (Margossian and Lowey, 1982). *Dictyostelium* full length myosin II and HMM-GFP were purified as described previously (Ruppel et al., 1994; Tokuraku et al., 2009). The HMM version of human myosin V with a FLAG-tag at the N-terminus and a c-myc tag at the C-terminus was coexpressed with calmodulin in insect cells and purified using a method described previously (Watanabe et al., 2006).

In our previous study, we used Rng2CHD fused with a His-tag at the N-terminus, and reported that His-Rng2CHD bundles actin filaments (Takaine et al., 2009). However, we subsequently discovered that the His tag enhances the affinity of Rng2CHD for actin filaments, and untagged Rng2CHD has very poor actin bundling activity while retaining actin binding activity (Figure Supplement 6). In this study, therefore, we used untagged Rng2CHD prepared as follows. The gene encoding Rng2CHD (Takaine et al., 2009) was inserted at the *Hind*III and *Pst*I sites of the pCold-TEV vector (Ngo et al., 2015), which had a TEV protease recognition sequence between the 6×His sequence and the multiple cloning site of pColdI (Takara Bio, Kusatsu, Japan). The amino acid sequence of His-TEV Rng2CHD was MNHKVHHHHHHIEGRHMENLYFQGTLEGSEFKLDVNVGL…(Rng2CHD)…LPNFKA, where the underline shows the TEV recognition sequence.

Rng2CHD was expressed in BL21 *Escherichia coli* (Takara Bio) according to the instructions provided by the manufacturer of pColdI. The cells were lysed by sonication in 2 mM 2-mercaptoethanol, 0.3% Triton X-100, 0.1 mM phenylmethylsulfonylfluoride, 400 mM NaCl, 10 mM imidazole (pH 7.4) and 20 mM Hepes (pH 7.4) on ice. The homogenate was clarified by centrifugation and mixed with Ni Sepharose 6 Fast Flow (GE Healthcare, Chicago, IL). After extensive washing, the peak fractions eluted by 7 mM 2-mercaptoethanol, 400 mM imidazole (pH 7.4) and 10 mM Hepes (pH 7.4) were combined and supplemented with His-tagged TEV protease at a 1/10 molar amount of proteins to separate the His-tag from Rng2CHD at the cleavage site for TEV protease. After dialysis against 50 mM KCl, 0.1 mM DTT and 10 mM Hepes (pH 7.4) overnight at 4°C, the protein solution was clarified by centrifugation and passed through Ni Sepharose 6 Fast Flow in a column to remove the released His-tag, His-TEV protease and uncleaved His-tagged Rng2CHD. This was followed by concentration with a centrifugal concentrator (Amicon Ultra-15 3 k device, Merck Millipore, Burlington, MA), and after supplementing with 10 mM DTT, aliquots were snap-frozen in liquid nitrogen and stored at -80°C.

To fuse GFP to the N-terminus of Rng2CHD, the GFP gene with a S65T mutation was inserted at the *Kpn*I and *BamH*I sites of pCold-TEV-Rng2CHD. A Gly-based 16 amino acid-residue

linker sequence was inserted between the GFP gene and the Rng2CHD gene, so that the expressed GFP would not spatially inhibit the binding of Rng2CHD to the actin filament. The resultant amino acid sequence of GFP-Rng2CHD was MNHKVHHHHHHIEGRHMENLYFQGTMSKGE…(GFP)…MDELYGGSEFGSSGSSGSSKLDV NVGL…(Rng2CHD)…LPNFKA, where the underline shows the TEV recognition sequence and the double underline shows the linker sequence. GFP-Rng2CHD was expressed in Rosetta DE3 *E. coli* (Merck Millipore), and purified basically in the same way as Rng2CHD, except that the protein was further purified by anion exchange chromatography with an Econo-pac High Q cartridge (BIO-RAD, Hercules, CA) before it was concentrated.

***In vitro* motility assays**

G-actin was polymerized in F-buffer (0.1 M KCl, 2 mM $MgCl_2$, 1 mM DTT, 1 mM ATP and 10 mM Hepes, pH 7.4) for 1 h at 22°C, and was diluted to 1 μM with NF buffer (25 mM KCl, 2 mM $MgCl_2$, 10 mM DTT and 20 mM Hepes, pH 7.4). Diluted actin filaments were incubated with 1 μM rhodamine phalloidin (Invitrogen, Waltham, MA) or 1 μM phalloidin (Wako, Osaka, Japan) for 1 h at 22°C.

In vitro actomyosin motility assays, in which actin filaments move on the HMM of skeletal muscle myosin II or full length *Dictyostelium* myosin II, were performed according to the method of Kron and Spudich (Kron and Spudich, 1986), using nitrocellulose-coated flow chambers. In the case of *Dictyostelium* myosin II, full length myosin in 10 mM Hepes, pH 7.4, 200 mM NaCl, 1 mM EDTA, 10 mM DTT was allowed to adhere to the surface, and then incubated with 0.5 mg/ml T166E recombinant myosin light chain kinase (Smith et al., 1996) for 5 min in NF buffer containing 0.5 mM ATP and 10 mg/ml BSA at room temperature. In the case of muscle HMM and myosin filaments, HMM in NF buffer or intact myosin II in 10 mM Hepes, pH 7.4, 50 mM NaCl, 4 mM $MgCl_2$, and 10 mM DTT was allowed to adhere to the nitrocellulose surface, followed by blocking with NF buffer containing 10 mg/mL BSA. Rhodamine phalloidin-stabilized actin filaments were then bound to myosin II on a nitrocellulose-coated glass surface in a flow chamber filled with NF buffer containing 10 mg/ml BSA. Movement of actin filaments was initiated by injecting twice the chamber volume of MA buffer (25 mM KCl, 2 mM $MgCl_2$, 10 mM DTT, 3 mg/ml glucose, 1.2 μM glucose oxidase, 0.15 μM catalase, 10 mg/ml BSA and 20 mM Hepes, pH 7.4) containing various concentrations of ATP, ADP and Rng2CHD, into the flow chamber. Fluorescence of rhodamine phalloidin was imaged with an EMCCD camera (iXon X3, Andor, Belfast, UK) on a fluorescent microscope (IX-71; Olympus, Tokyo, Japan) equipped with a Plan Apo 100X, 0.9 NA objective lens (Nikon) at a frame rate of 4 fps. The images were processed with Image J (Schneider et al., 2012). For each condition, more than 100 filaments longer than 1.5 μm were randomly selected, and their movements were tracked by MTrackJ, a plugin for Image J (Meijering et al., 2012).

The actomyosin II motility assay in the presence of GFP-Rng2CHD was performed basically as indicated above, with several modifications. Rhodamine phalloidin-stabilized and unlabeled phalloidin-stabilized actin filaments were mixed at a 1:1 concentration in order to observe GFP fluorescence without the interference of rhodamine fluorescence. Fluorescence micrographs were taken with an EMCCD camera (iXon X3) on a TIRF microscope (IX-71) equipped with a UApo N 100X, 1.49 NA objective lens (Olympus). Laser light of 538 nm for exciting rhodamine and 488 nm for exciting GFP were irradiated alternately at 2 s intervals, and the time-lapse imaging of moving actin filaments and GFP-Rng2CHD dynamics was performed semi-simultaneously. The fluorescence intensity of GFP was quantified by Image J as follows. Five filaments near the center of the images were selected for each condition, and the fluorescence intensity in five frames was measured. The light intensity at five points near the filament was averaged and subtracted from the measured values along the filament as the background for each filament. The values were normalized by the length of each filament.

For *in vitro* motility assays in which actin filaments move on myc-tagged myosin V HMM, HMM molecules were immobilized on a glass surface via anti-c-myc antibody. MA2 buffer (20 mM KCl, 4 mM $MgCl_2$, 2 mM ATP, 120 μM calmodulin, 1 mM EGTA, 1 mM DTT, 0.5% methylcellulose, 1 mg/ml BSA and 25 mM imidazole, pH 7.4) was used instead of MA buffer. Mouse calmodulin was expressed in *E. coli* and purified as described previously (Shishido et al., 2009). Fluorescence images were captured with a camera (ORCA-Flash 2.8; Hamamatsu Photonics, Hamamatsu, Japan) on a fluorescent microscope (IX-70; Olympus) equipped with a Plan-Fluor 100X, 1.3 NA objective lens (Nikon, Tokyo, Japan) at a frame rate of 0.5 fps.

Measurement of dissociation constant

G-actin was polymerized in F-buffer for 1 h at 22°C and incubated with phalloidin at a 1:1 molar ratio for 1 h at 22°C. Phalloidin-stabilized actin filaments that were diluted to 3 μM and various concentrations of Rng2CHD or GFP-Rng2CHD (1, 2, 3, 4, 5, 6 μM) were incubated together in SA buffer (25 mM KCl, 2 mM $MgCl_2$, 0.5 mM ATP, 10 mM DTT and 20 mM Hepes, pH 7.4) for 5 min at 22°C, and then centrifuged at 278,800 g for 10 min at 22°C. The supernatants and pellets were subjected to SDS-PAGE. Images of Coomassie brilliant blue (CBB)-stained gels were read into Image J and the concentration of Rng2CHD in each fraction was quantified by densitometry. The dissociation constant (K_d) for Rng2CHD to actin filaments was calculated by fitting plots of [Rng2CHD bound to actin filaments] versus [Rng2CHD free] with the following equation:

$$[Rng2CHD_{bound}] = [Actin_{total}]\,[Rng2CHD_{free}] / ([Rng2CHD_{free}]+K_d) \quad [1]$$

K_d between actin filaments and GFP-Rng2CHD was calculated in the same way.

Estimation of binding ratio of Rng2CHD and GFP-Rng2CHD to actin filament from K_d

K_d between Rng2CHD and actin filaments is given by:

$$K_d = [Actin_{free}]\,[Rng2CHD_{free}] / [Rng2CHD_{bound}] \quad [2]$$

The concentration of actin filaments is extremely low in flow chambers in which Rng2CHD in the buffer interacts with actin filaments immobilized on the substrate and unbound actin filaments were washed away, such as *in vitro* actomyosin motility assays and observations of binding by fluorescence microscopy. Under those conditions, $[Rng2CHD_{free}]$ can be approximated by the concentration of total Rng2CHD ($[Rng2CHD_{total}]$). Therefore, the following approximation holds from Eq. 2:

$$[Rng2CHD_{bound}] / [Actin_{free}] \simeq [Rng2CHD_{total}] / K_d \quad [3]$$

The binding ratios of Rng2CHD and GFP-Rng2CHD to the dilute actin protomers were estimated with this approximation using the value of K_d.

In HS-AFM imaging to measure HHP, unbound actin filaments in solution did not interfere with the imaging, and therefore we were able to include a defined concentration of actin in the observation buffer. In those experiments, the binding ratio was calculated from eq [1].

High-speed atomic force microscopy

We used a laboratory-built high-speed atomic microscope (HS-AFM) as described previously (Ando et al., 2013). HS-AFM imaging in the amplitude modulation tapping mode was carried out in solution with small cantilevers (BL-AC10DS-A2, Olympus) whose spring constant, resonant frequency in water, and quality factor in water were ~0.1 N/m, ~500 kHz, and ~1.5, respectively. An additional tip was grown, in gas supplied from sublimable ferrocene powder, on the original cantilever tip by electron beam deposition (EBD) using scanning electron microscopy (ZEISS Supra 40 VP/Gemini column, Zeiss, Jena, Germany). Typically, the EBD tip was grown under vacuum (1 - 5 x 10^{-6} Torr), an aperture size of 10 µm, and electron beam voltage of 20 keV for 30 s. The EBD ferrocene tip was further sharpened using a radio frequency plasma etcher (Tergeo Plasma Cleaner, Pie Scientific, Union City, CA) under an argon gas atmosphere (typically at 180 mTorr and 20 W for 30 s). For HS-AFM imaging, the free-oscillation peak-to-peak amplitude of the cantilever (A_0) was set at ~1.6 - 1.8 nm, and the feedback amplitude set-point was set at ~0.9 A_0.

Liposomes composed of DPPC/DPTAP (90/10, wt/wt) and mica-supported lipid bilayer were made according to our previous sample preparation protocol (Ngo et al., 2015). We used this positively charged lipid bilayer for gently immobilizing actin filaments in all HS-AFM experiments. In the first set of experiments, we observed the impact of different Rng2CHD binding ratios on the structure of actin filaments at the equilibrium binding states between Rng2CHD and actin filaments. Actin filaments were initially made at a final actin concentration of 20 µM in F-buffer containing 0.1 M KCl, 2 mM MgCl2, 1 mM DTT, 1 mM ATP and 10 mM Hepes-KOH pH 7.4 for ~1 h at 22°C. For HS-AFM imaging of actin filaments at different Rng2CHD binding ratios, we fixed the final

concentration of actin filaments in the AFM observation chamber at 0.59 µM in the observation buffer (25 mM KCl, 2 mM $MgCl_2$, 50 µM ATP, 1 mM ADP, 10 mM DTT, and 20 mM Hepes pH 7.4) and calculated the binding ratios at different concentrations of Rng2CHD using a K_d of 0.92 µM (Table Supplement 1). The protein bindings were allowed after an incubation of the mixture in a tube at 22°C for 10 min or longer. The protein mixture (68 µl) was added into the observation chamber, in which the positively charged lipid bilayer was already made, followed by the approaching process of the sample scanner stage. The actin filaments at different Rng2CHD binding ratios were gently immobilized onto this lipid bilayer during sample approaching (~5-7 min), prior to the HS-AFM imaging. HS-AFM imaging process was performed as described in detail elsewhere (Ando et al., 2013), except an additional use of a recently developed OTI mode (Fukuda et al., 2021). Half helical pitches (HHPs) of actin filaments were analyzed by measuring the distance between the crossover points of two single actin protofilaments along the filaments using a home-built software (UMEX Viewer for Drift Analysis), which allowed us to semi-automatically determine and measure the distance between highest points of two neighboring actin protomers (e.g., HHPs) by making a topographical line profile along actin filaments. Briefly, a cross-sectional profile line was drawn along the long axis of the actin filament with the length of 1 – 3 consecutive half helices. Prior to the analysis, the nonlinearity of the XY piezos was corrected by a nonlinear image scaling, and the image noise was suppressed by a Gaussian smooth filter with the standard deviation of 0.76 nm. The profile was extracted by averaging the signal in a 6 nm band along the filament. To reduce the effect of noise, we set minimum threshold pitch values of 3 and 20 nm for the actin protomer and HHP, respectively. The measured HHP data were copied into an Excel datasheets for statistical analysis.

In the second set of experiments, we analyzed the impact of Rng2CHD on the binding of S1 to actin filaments. G-actin was polymerized in F-buffer for 1 h at 22°C, and then the buffer on the sample stage was replaced by 2 µl of 20 µM actin filaments in HSAFM buffer (25 mM KCl, 2 mM $MgCl_2$, 50 µM ATP, 1 mM ADP, 10 mM DTT, 20 mM Hepes, pH 7.4). After incubation for 10 min at 22°C, the surface of the sample stage was rinsed with 20 µl of HSAFM buffer to remove free actin filaments. Subsequently, the surface of the sample stage was immersed in 60 µl of HSAFM buffer in the observation chamber of the HS-AFM. Observations of the transient binding of muscle S1 to actin filaments in the presence of ATP and ADP were performed under the following two conditions: (1) S1 diluted in HSAFM buffer was added to the observation chamber to a final concentration of 500 nM; (2) 12 nM Rng2CHD was allowed to interact with actin filaments in the observation chamber for 15 min at 22°C, and then 20 µM S1 in HSAFM buffer was added to the observation chamber to a final concentration of 500 nM. AFM images were obtained at a scan speed of 0.5 s per field of view, and were then visualized by Kodec4, our laboratory-built software (Ngo et al., 2015). Images scanned between 1 min and 2 min after the addition of S1 or ATP were analyzed, and the events of transient binding of S1 molecules to actin filaments were visually counted.

766

767 **Electron microscopy**

768 G-actin was polymerized in F-buffer for 1 h at room temperature, and 1 μM actin filaments were
769 mixed with various concentrations of Rng2CHD in EM buffer (25 mM KCl, 4 mM $MgCl_2$, 1 mM
770 DTT, 0.1 mM ATP and 10 mM imidazole, pH 7.4) at room temperature. A small volume of each
771 sample was placed on a carbon-coated grid for 30 s (40 nM Rng2CHD), 2 min (200 nM Rng2CHD)
772 or 4 min (1 μM Rng2CHD) after mixing. The samples were negatively stained with 1% uranyl
773 acetate, and observed in a transmission electron microscope (Tecnai F20; FEI, Hillsboro, OR).
774 Electron micrographs were recorded with a Gatan ORIUS 831 CCD camera (Pleasanton, CA),
775 adjusted for contrast and Gaussian-filtered using Adobe Photoshop.

776

777 **Myosin II S1 ATPase measurements**

778 Actin-activated S1 ATPase was measured using malachite green (Kodama et al., 1986). G-actin was
779 polymerized in F-buffer for 1 h at 22°C. The solution was centrifuged at 278,800 g for 10 min at
780 22°C and actin filaments in the pellet were resuspended in NF buffer. This procedure was repeated
781 once more to minimize the amount of carried-over phosphate. Actin filaments and various
782 concentrations of Rng2CHD (0, 0.33, 0.82, 1.9, 5.0 μM) were mixed in NF buffer containing 2 mM
783 ATP, then incubated for 10 min at 25°C. The reaction was started by the addition of S1, and
784 phosphate released at 0, 2, 4, 6 and 8 min was measured. The final concentrations of actin and S1
785 were 24 μM and 50 nM, respectively.

786

787 **Co-sedimentation assay of actin filaments and S1 with Rng2CHD**

788 For the co-sedimentation assays in the presence of ATP, G-actin was polymerized in F-buffer for 1 h
789 at 22°C, then incubated with phalloidin at a 1:1 molar ratio for 1 h at 22°C. For the co-sedimentation
790 assays in the presence of ADP, the solution of actin filaments was centrifuged at 278,800 g for 10
791 min at 22°C, and the pelleted actin filaments were resuspended in NF buffer. This procedure was
792 repeated once again to minimize the amount of carried-over ATP before the addition of phalloidin.
793 The following two samples were prepared for both experiments: (1) 3 μM actin filaments were
794 incubated with 2 μM S1 for 5 min at 22°C; (2) 3 μM actin filaments were incubated with 2 μM
795 Rng2CHD for 10 min at 22°C, and after adding S1, were incubated for 5 min at 22°C. Each sample
796 was prepared in S-ATP buffer (25 mM KCl, 2 mM $MgCl_2$, 2 mM ATP, 10 mM DTT, 10 mM
797 phosphoenolpyruvate, 10 units/ml pyruvate kinase and 20 mM Hepes, pH 7.4) or S-ADP buffer (25
798 mM KCl, 2 mM $MgCl_2$, 2 mM ADP, 10 mM DTT and 20 mM Hepes, pH 7.4). After incubation,
799 each sample was centrifuged at 278,800 g for 10 min at 22°C. The supernatants and pellets were
800 subjected to SDS-PAGE. Images of CBB-stained gels were read by and into Image J and the
801 concentration of S1 in each fraction was quantified by densitometry.

Fluorescence microscope-based binding assay

Binding of HMM-GFP to actin filaments was observed as follows. G-actin was polymerized in FF-buffer (50 mM KCl, 2 mM $MgCl_2$, 0.5 mM EGTA, 1 mM DTT, 20 mM PIPES, pH 6.5) containing 0.2 mM ATP for 2 h at 22°C. Actin filaments and Alexa 647 phalloidin (Invitrogen) were mixed at a molar ratio of 20:1 and incubated overnight on ice. The surface of each coverslip was covered with a positively charged lipid bilayer and was used to construct flow chambers as described previously (Ngo et al., 2015), except that the weight ratio of 1,2-dipalmitoyl-sn-glycero-3-phosphocholine (DPPC; Avanti Polar Lipids, Alabaster, AL) and 1,2-dipalmitoyl-3-trimethylammonium-propane (DPTAP; Avanti Polar Lipids) was 17:3 (Hirakawa et al., 2017; Hosokawa et al., 2021). Alexa 647 phalloidin-stabilized actin filaments diluted in FF-ATP buffer (FF buffer containing 0.5 μM ATP) were introduced into the flow chamber to loosely bind to the positively charged lipid layer. HMM-GFP and Rng2CHD diluted in FF-ATP buffer were then introduced to the flow chamber. Alternatively, FF-ATP buffer in the above procedures was replaced with FF buffer for the assays in the nucleotide-free state. Fluorescence of Alexa 647 and GFP was imaged with a fluorescence microscope (ECLIPSE E600, Nikon) equipped with an ARUGUS-HiSCA system (Hamamatsu Photonics). Images were captured using a 100x objective lens (CFI Plan Apo Lambda 100x Oil, NA 1.45; Nikon).

Acknowledgments

We thank Dr. Atsuko H. Iwane and Dr. Toshio Yanagida for the gift of the virus to express HMM of myosin V. This work was supported in part by Bio-SPMs Collaborative Research of WPI Nano Life Science Institute, Kanazawa University, and Grants-in-aid from the Ministry of Education, Culture, Sports, Science and Technology to KT (No. 24370069 and 24117008), KN (No. 22019004), MT (No. 24770177) and TU (No. 24370069 and 24117008).

Author contributions

NK, KT, ON, TF, TA, KN and TU conceived and supervised the study, YH, MT, KXN, KT, KN and TU designed the experiments, YH, MT, KXN, TI, MY, ABB,KH, AY and TU performed the experiments, YH, MT, KXN, MY, ABB, KU, KH and TU analyzed the data, YH and TU wrote the manuscript draft and KXN, KH, NK, KT, TF, MT and KN revised the manuscript.

Conflicts of interest

The authors declare no conflicts of interest.

Videos (the video files can be downloaded at https://www.dropbox.com/sh/r1qvgkjlxjzzvxk/AAACHWH0ZeRzxgnW1eemp2qGa?dl=0)

Video 1. Movement of actin filaments on surfaces coated with full length *Dictyostelium* myosin II in the absence (left) or the presence of 200 nM (middle) and 1 μM (right) Rng2CHD. The concentration of ATP was 1 mM. Playing speed is 1x.

Video 2. Movement of actin filaments on surfaces coated with HMM of rabbit skeletal muscle myosin II in the absence (left) or the presence of 50 nM (middle) and 200 nM (right) Rng2CHD. The concentration of ATP was 1 mM. Playing speed is 1x.

Video 3. Movement of actin filaments on surfaces coated with filaments of rabbit skeletal muscle myosin II in the absence (left) or presence of 100 nM Rng2CHD (right). The concentration of ATP was 0.5 mM. Playing speed is 1x.

Video 4. Movement of actin filaments on surfaces coated with HMM of rabbit skeletal muscle myosin II in the presence of 200 nM Rng2CHD and in the presence of 1 mM ATP (left) or 0.2 mM ATP and 1 mM ADP (right). Playing speed is 7.5x.

Video 5. Movement of actin filaments on surfaces coated with HMM of mouse myosin V in the absence (left) or the presence of 330 nM Rng2CHD (rigbt) Rng2CHD. The concentration of ATP was 2 mM. Playing speed is 1x.

Video 6. Transient binding of Rng2CHD. Real time HS-AFM observation of 0.59 μM actin filaments interacting with 0, 0.25, 0.85 and 5.7 μM Rng2CHD. The estimated binding ratios under those conditions are 0, 15%, 40% and 85%, respectively. Red and green arrowheads denote sparse binding of Rng2CHD molecules and some typical Rng2CHD clusters, respectively. Imaging rate was 2 frame/s and the playing speed is 15x. Bars: 25 nm. For details, see Figure 4.

Video 7. Distortion of helical structures of actin filaments and separation of protofilaments induced by high concentration of Rng2CHD. Imaging rate was 1 frame/s, and the playing speed is 10x. Bars: 25 nm. For details, see Figure Supplement 3.

References

Ando T, Uchihashi T, Kodera N. 2013. High-Speed AFM and Applications to Biomolecular Systems. *Annu Rev Biophys* **42**:393–414. doi:10.1146/annurev-biophys-083012-130324

Clarke M, Spudich JA. 1977. Nonmuscle Contractile Proteins: The Role of Actin and Myosin in Cell Motility and Shape Determination. *Annu Rev Biochem* **46**:797–822. doi:10.1146/annurev.bi.46.070177.004053

Cooke R, Crowder MS, Wendt CH, Barnett VA, Thomas DD. 1984. Muscle Cross-Bridges: Do They Rotate? *Adv Exp Med Biol* **170**:413–427. doi:10.1007/978-1-4684-4703-3_37

Ebashi S, Kodama A. 1966. Interaction of Troponin with F-Actin in the Presence of Tropomyosin. *J Biochem* **59**:425–426. doi:10.1093/oxfordjournals.jbchem.a128320

Ebashi S, Kodama A. 1965. A new protein factor promoting aggregation of tropomyosin. *J Biochem* **58**:107–108. doi:10.1016/S0006-291X(08)00430-0

Eng K, Naqvi NI, Wong KCY, Balasubramanian MK. 1998. Rng2p, a protein required for cytokinesis in fission yeast, is a component of the actomyosin ring and the spindle pole body. *Curr Biol* **8**:611–621. doi:10.1016/S0960-9822(98)70248-9

Galkin VE, Orlova A, Lukoyanova N, Wriggersd W, Egelman EH. 2001. Actin depolymerizing factor stabilizes an existing state of F-actin and can change the tilt of F-actin subunits. *J Cell Biol* **153**:75–86. doi:10.1083/jcb.153.1.75

Goyal A, Takaine M, Simanis V, Nakano K. 2011. Dividing the spoils of growth and the cell cycle: The fission yeast as a model for the study of cytokinesis. *Cytoskeleton* **68**:69–88. doi:10.1002/cm.20500

Griffith LM, Downs SM, Spudich JA. 1987. Myosin light chain kinase and myosin light chain phosphatase from Dictyostelium: Effects of reversible phosphorylation on myosin structure and function. *J Cell Biol* **104**:1309–1323. doi:10.1083/jcb.104.5.1309

Harris AR, Jreij P, Belardi B, Joffe AM, Bausch AR, Fletcher DA. 2020. Biased localization of actin binding proteins by actin filament conformation. *Nat Commun* **11**:1–13. doi:10.1038/s41467-020-19768-9

Higashi-Fujime S. 1983. Phosphorylation of myosin light chain modulates the in vitro movement of fibrils composed of actin and myosin filaments from skeletal muscle. *J Biochem* **94**:1539–1545.

Hirakawa R, Nishikawa Y, Uyeda TQP, Tokuraku K. 2017. Unidirectional growth of heavy meromyosin clusters along actin filaments revealed by real-time fluorescence microscopy. *Cytoskeleton* **74**:482–489. doi:10.1002/cm.21408

Huxley AF, Niedergerke R. 1954. Structural Changes in Muscle During Contraction: Interference Microscopy of Living Muscle Fibres. *Nature* **173**:971–973. doi:10.1038/173971a0

Huxley H, Hanson J. 1954. Changes in the Cross-Striations of Muscle during Contraction and Stretch and their Structural Interpretation. *Nature* **173**:973–976.

Huxley HE. 1969. The Mechanism of Muscular Contraction. *Science* **164**:1356–1366.

doi:10.1126/science.164.3886.1356

Khaitlina S, Tsaplina O, Hinssen H. 2017. Cooperative effects of tropomyosin on the dynamics of the actin filament. *FEBS Lett* **591**:1884–1891. doi:10.1002/1873-3468.12700

Kodama T, Fukui K, Kometani K. 1986. The initial phosphate burst in ATP hydrolysis by myosin and subfragment-1 as studied by a modified malachite green method for determination of inorganic phosphate. *J Biochem* **99**:1465–1472. doi:10.1093/oxfordjournals.jbchem.a135616

Korn ED. 1978. Biochemistry of actomyosin-dependent cell motility (A review). *Proc Natl Acad Sci U S A* **75**:588–599. doi:10.1073/pnas.75.2.588

Kron SJ, Spudich JA. 1986. Fluorescent actin filaments move on myosin fixed to a glass surface. *Proc Natl Acad Sci U S A* **83**:6272–6276. doi:10.1073/pnas.83.17.6272

Kubota H, Mikhailenko S V., Okabe H, Taguchi H, Ishiwata S. 2009. D-loop of actin differently regulates the motor function of myosins II and V. *J Biol Chem* **284**:35251–35258. doi:10.1074/jbc.M109.013565

Lymn RW, Taylor EW. 1971. Mechanism of Adenosine Triphosphate Hydrolysis by Actomyosin. *Biochemistry* **10**:4617–4624. doi:10.1021/bi00801a004

Mabuchi I, Okuno M. 1977. The effect of myosin antibody on the division of starfish blastomeres. *J Cell Biol* **74**:251–263. doi:10.1083/jcb.74.1.251

Margossian SS, Lowey S. 1982. Preparation of myosin and its subfragments from rabbit skeletal muscle. *Methods Enzymol* **85**:55–71. doi:10.1016/0076-6879(82)85009-X

McGough A, Pope B, Chiu W, Weeds A. 1997. Cofilin changes the twist of F-actin: Implications for actin filament dynamics and cellular function. *J Cell Biol* **138**:771–781. doi:10.1083/jcb.138.4.771

Meijering E, Dzyubachyk O, Smal I. 2012. Methods for Cell and Particle Tracking. *Methods Enzymol* **504**:183–200. doi:10.1016/B978-0-12-391857-4.00009-4

Miki M, Wahl P, Auchet J. 1982. Fluorescence anisotropy of labeled F-actin: influence of divalent cations on the interaction between F-actin and myosin heads. *Biochemistry* **21**:3661–3665. doi:10.1021/bi00258a021

Mukhina S, Wang Y, Murata-Hori M. 2007. Alpha-Actinin is Required for Tightly Regulated Remodeling of the Actin Cortical Network during Cytokinesis. *Dev Cell* **13**:554–565. doi:10.1016/j.pestbp.2011.02.012.Investigations

Ngo KX, Kodera N, Katayama E, Ando T, Uyeda TQP. 2015. Cofilin-induced unidirectional cooperative conformational changes in actin filaments revealed by high-speed atomic force microscopy. *eLife* **4**:1–19. doi:10.7554/eLife.04806

Ngo KX, Umeki N, Kijima ST, Kodera N, Ueno H, Furutani-Umezu N, Nakajima J, Noguchi TQP, Nagasaki A, Tokuraku K, Uyeda TQP. 2016. Allosteric regulation by cooperative conformational changes of actin filaments drives mutually exclusive binding with cofilin and myosin. *Sci Rep* **6**:1–11. doi:10.1038/srep35449

940 Noguchi TQP, Komori T, Umeki N, Demizu N, Ito K, Iwane AH, Tokuraku K, Yanagida T, Uyeda TQP.
941 2012. G146V mutation at the hinge region of actin reveals a myosin class-specific requirement of
942 actin conformations for motility. *J Biol Chem* **287**:24339–24345. doi:10.1074/jbc.M111.321752
943 Oosawa F, Fujime S, Ishiwata S, Mihashi K. 1973. Dynamic Property of F-Actin and Thin Filament. *Cold*
944 *Spring Harb Symp Quant Biol* **37**:277–285. doi:10.1101/sqb.1973.037.01.038
945 Orlova A, Prochniewicz E, Egelman EH. 1995. Structural Dynamics of F-Actin: II. Cooperativity in
946 Structural Transitions. *J Mol Biol* **245**:598–607. doi:10.1006/jmbi.1994.0049
947 Papp G, Bugyi B, Ujfalusi Z, Barkó S, Hild G, Somogyi B, Nyitrai M. 2006. Conformational changes in
948 actin filaments induced by formin binding to the barbed end. *Biophys J* **91**:2564–2572.
949 doi:10.1529/biophysj.106.087775
950 Pardee JD, Spudich JA. 1982. Purification of muscle actin. *Methods Enzymol* **85**:164–181.
951 doi:10.1016/0076-6879(82)85020-9
952 Pollard TD. 2010. Mechanics of cytokinesis in eukaryotes. *Curr Opin Cell Biol* **22**:50–56.
953 doi:10.1016/j.ceb.2009.11.010.
954 Pollard TD, Weihing RR, Adelman MR. 1974. Actin and myosin and cell movement. *CRC Crit Rev*
955 *Biochem* **2**:1–65. doi:10.3109/10409237409105443
956 Prochniewicz E, Chin HF, Henn A, Hannemann DE, Olivares AO, Thomas DD, De La Cruz EM. 2010.
957 Myosin Isoform Determines the Conformational Dynamics and Cooperativity of Actin Filaments in
958 the Strongly Bound Actomyosin Complex. *J Mol Biol* **396**:501–509. doi:10.1016/j.jmb.2009.11.063
959 Ritchie MD, Geeves MA, Woodward SKA, Manstein DJ. 1993. Kinetic characterization of a cytoplasmic
960 myosin motor domain expressed in Dictyostelium discoideum. *Proc Natl Acad Sci U S A* **90**:8619–
961 8623. doi:10.1073/pnas.90.18.8619
962 Ruppel KM, Uyeda TQP, Spudich JA. 1994. Role of highly conserved lysine 130 of myosin motor
963 domain. In vivo and in vitro characterization of site specifically mutated myosin. *J Biol Chem*
964 **269**:18773–18780. doi:10.1016/s0021-9258(17)32235-4
965 Satterwhite LL, Pollard TD. 1992. Cytokinesis. *Curr Opin Cell Biol* **4**:43–52. doi:10.1016/0955-
966 0674(92)90057-J
967 Schneider CA, Rasband WS, Eliceiri KW. 2012. NIH Image to ImageJ: 25 years of Image Analysis HHS
968 Public Access. *Nat Methods* **9**:671–675. doi:10.1038/nmeth.2089
969 Sellers JR, Spudich JA, Sheetz MP. 1985. Light chain phosphorylation regulates the movement of smooth
970 muscle myosin on actin filaments. *J Cell Biol* **101**:1897–1902. doi:10.1083/jcb.101.5.1897
971 Shibata K, Nagasaki A, Adachi H, Uyeda TQP. 2016. Actin binding domain of filamin distinguishes
972 posterior from anterior actin filaments in migrating Dictyostelium cells. *Biophys Physicobiology*
973 **13**:321–331. doi:10.2142/biophysico.13.0
974 Shirinsky VP, Biryukov KG, Hettasch JM, Sellers JR. 1992. Inhibition of the relative movement of actin
975 and myosin by caldesmon and calponin. *J Biol Chem* **267**:15886–15892.

Shishido H, Yamada MD, Kondo K, Maruta S. 2009. Photocontrol of calmodulin interaction with target peptides using azobenzene derivative. *J Biochem* **146**:581–590. doi:10.1093/jb/mvp107

Singh I, Goll DE, Robson RM. 1981. Effect of α-actinin on actin structure Actin ATPase activity. *Biochim Biophys Acta - Protein Struct* **670**:1–8. doi:10.1016/0005-2795(81)90041-6

Smith JL, Silveira LA, Spudich JA. 1996. Activation of dictyostelium myosin light chain kinase A by phosphorylation of Thr166. *EMBO J* **15**:6075–6083. doi:10.1002/j.1460-2075.1996.tb00996.x

Spudich JA, Watt S. 1971. The Regulation of Rabbit Skeletal Muscle Contraction. *J Biol Chem* **246**:4866–4871. doi:10.3233/SAV-2010-0562

Takaine M, Numata O, Nakano K. 2009. Fission yeast IQGAP arranges actin filaments into the cytokinetic contractile ring. *EMBO J* **28**:3117–3131. doi:10.1038/emboj.2009.252

Tebbs IR, Pollard TD. 2013. Separate roles of IQGAP Rng2p in forming and constricting the Schizosaccharomyces pombe cytokinetic contractile ring. *Mol Biol Cell* **24**:1904–1917. doi:10.1091/mbc.E12-10-0775

Tokunaga M. 1991. Structure and structural change of the myosin head. *Adv Biophys* **27**:157–167. doi:10.1016/0065-227X(91)90015-6

Tokuraku K, Kurogi R, Toya R, Uyeda TQP. 2009. Novel Mode of Cooperative Binding between Myosin and Mg^{2+}-actin Filaments in the Presence of Low Concentrations of ATP. *J Mol Biol* **386**:149–162. doi:10.1016/j.jmb.2008.12.008. Epub 2008 Dec 11

Toyoshima YY, Kron SJ, Spudich JA. 1990. The myosin step size: Measurement of the unit displacement per ATP hydrolyzed in an in vitro assay. *Proc Natl Acad Sci U S A* **87**:7130–7134. doi:10.1073/pnas.87.18.7130

Uyeda TQP, Abramson PD, Spudich JA. 1996. The neck region of the myosin motor domain acts as a lever arm to generate movement. *Proc Natl Acad Sci U S A* **93**:4459–4464. doi:10.1073/pnas.93.9.4459

Uyeda TQP, Kron SJ, Spudich JA. 1990. Myosin step size: estimation from slow sliding movement of actin over low densities of heavy meromyosin. *J Mol Biol* **214**:699–710. doi:10.1016/0022-2836(90)90287-V

Watanabe S, Ikebe R, Ikebe M. 2006. Drosophila myosin VIIA is a high duty ratio motor with a unique kinetic mechanism. *J Biol Chem* **281**:7151–7160. doi:10.1074/jbc.M511592200

Supplementary Materials

Supplementary information 1. Estimation of binding ratio of GFP-Rng2CHD along actin filaments based on *Kd*.

Densitometric scanning of a cosedimentation gel shown in Figure 3D resulted in the binding curve shown below. Fitting of the data points, shown in dotted line, yielded the K_d value of 3.4 μM.

The table below shows the binding densities of Rng2CHD needed to achieve several degrees of motility inhibition on muscle HMM, calculated based on K_d (for Rng2CHD and GFP-Rng2CHD) and also directly from the fluorescence intensities of GFP-Rng2CHD.

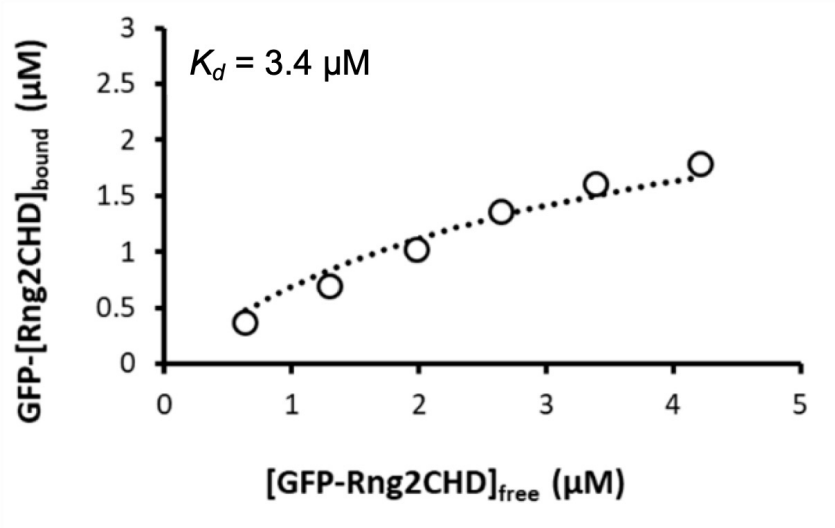

Table. Binding ratio of Rng2CHD needed to achieve various degrees of motility inhibition*

Degree of inhibition		50%	75%	80%	90%	95%
Rng2CHD	Based on K_d	1.3%	3.3%	3.6%	4.8%	7.7%
GFP-Rng2CHD**	Based on K_d	4.3%	6.7%	7.1%	13%	20%
	GFP-fluorescence	nd	nd	9.7%	21%	nd

*: Effects of Rng2CHD on motility of actin filaments on muscle HMM were assayed in several independent sets of experiments under different conditions. The data shown here were measured in the presence of 0.5 mM ATP, which is different from those shown in Figure 1.

**: The estimated binding ratios of GFP-Rng2CHD needed to achieve the same degree of inhibition was slightly lower when estimated from K_d than directly measured from the fluorescence intensities. However, both methods of estimation yielded higher required binding ratios than Rng2CHD, suggesting that the fused GFP moiety interferes with the activity of Rng2CHD to inhibit the motility of actin filaments on muscle HMM. nd: not determined.

Supplementary information 2. Possible mechanisms for differential responses of skeletal muscle myosin II and *Dictyostelium* non-muscle myosin II to Rng2CHD.

Although actin movements by both skeletal muscle and *Dictyostelium* myosin IIs were inhibited by Rng2CHD, the apparent modes of inhibition were very different. On muscle myosin II-coated surfaces, actin movements were inhibited by relatively low concentrations of Rng2CHD and were virtually immobilized at 200 nM Rng2CHD (Figure 1A, Video 2 and Figure Supplement 1). In contrast, actin filaments moving on *Dictyostelium* myosin II-coated surfaces appeared to lose affinity with the surface in the presence of medium concentrations of Rng2CHD without slowing significantly, and they diffused away from the surface in the presence of high concentrations of Rng2CHD (Figure 1B and 1C and Video 1). This apparent difference can be explained, at least in part, by two quantitative differences between muscle and *Dictyostelium* myosin IIs within the framework that Rng2CHD impairs the generation of active force by affecting the transition from the A•M•ADP•Pi complex to the A•M•ADP complex and/or the affinity of the A•M•ADP complex.

The first quantitative difference is the affinity for actin in the so-called weakly bound state. *Dictyostelium* myosin II has only three positive charges in loop 2, while muscle myosin II has five. Loop 2 is a major electrostatic actin binding site in the weakly bound state, and the number of positive charges in loop 2 determines the affinity for actin in the weakly bound state (Furch et al., 1996). The resistive load by increasing the number of weakly-bound muscle myosin II motors has been shown to slow and ultimately stop the movement propelled by active muscle HMM (Warshaw et al., 1990). In contrast, the weaker affinity of *Dictyostelium* myosin II in the weakly bound state would lead to smaller resistive load, which could result in an apparently very different outcome when the generation of active force is reduced by Rng2CHD. Moreover, the weaker weakly bound state with *Dictyostelium* myosin II would allow the actin filaments to detach from the myosin-coated surface when tethering by strongly-bound force-generating interactions is shortened or weakened by Rng2CHD.

The second quantitative difference that could contribute to the apparent difference in sensitivities of the two myosin IIs to Rng2CHD is the longer duration of the strongly-bound, force-generating A•M•ADP complex of *Dictyostelium* myosin II, and this mechanism is supported by the fact that the movement by muscle HMM became less sensitive to Rng2CHD in the presence of 0.2 mM ATP and 1 mM ADP (Figure 1B, Video 3 and Figure Supplement 1). We presume that in the presence of intermediate concentrations of Rng2CHD (i.e., 100-200 nM), many, but not all, of the productive force-generating events are inhibited, so that the remainder of the productive interactions are insufficient to move actin filaments against the resistive load imposed by weakly-bound crossbridges of muscle myosin II. However, the small number of force-generating crossbridges may be sufficient to move actin slowly when duration of the tension-bearing A•M•ADP complexes is extended. In the case of *Dictyostelium* myosin II, the resistive load by weakly-bound crossbridges is

smaller, and the duration of the tension-bearing A•M•ADP complexes is longer, so that Rng2CHD-affected actin filaments move on *Dictyostelium* myosin II without slowing significantly, and eventually detach from the myosin-coated surfaces.

Rng2CHD-induced weaker affinity of the A•M•ADP complex could have an interesting consequence in the case of *Dictyostelium* myosin II. Shortening of the lifetime of the affected A•M•ADP complexes may accelerate the movement within a certain range of Rng2CHD concentrations when the ensemble of the active force is sufficient to overcome the resistive load. This may be the reason why the average actin velocity was slightly faster in the presence of 50 nM Rng2CHD than in its absence (Figure 1B).

Although the combination of the above two quantitative differences can explain, at least in part, the observed apparent difference in the response of the two myosin IIs to Rng2CHD, we cannot rule out the possibility that the Rng2CHD affects the motilities of muscle and *Dictyostelium* myosin IIs in a manner not easily predicted within the framework of the standard swinging lever-arm model.

Supplementary information 3. Comparison of the actin sliding speed by myosin II *in vitro*, and the contraction speed of contractile rings *in vivo*.

The contraction speed of contractile rings (CRs) is much slower than the sliding velocity of actomyosin II *in vitro*. For instance, CRs in *S. pombe* contract at a rate of 0.5 μm/min circumferentially (Pelham and Chang, 2002), while actin filaments on *S. pombe* myosin II-coated surfaces move at a rate of 30 μm/min *in vitro* (Lord and Pollard, 2004). In *Dictyostelium*, the circumferential contraction velocity of the CR is 0.18 μm/s (Zang et al., 1997), whereas the sliding velocity of actin filaments on *Dictyostelium* myosin II is 1.1 μm/s (Figure 1B) or 1.4 μm/s (Kron and Spudich, 1986) *in vitro*, more than 5-fold faster than the circumferential speed of CR contraction.

A direct comparison of *in vitro* sliding speed and contraction speed is difficult for two reasons. The first aspect to complicate the quantitative comparison of the two speeds is the geometry of CRs. In the case of the simplest model CR that consists of a single contractile unit, shown below, the circumference of the CR would contract at 2x the speed of unitary actomyosin sliding speed. If CR consists of a series of multiple contractile units, as would be expected for real CRs, the circumferential speed of contraction would be further multiplied by the number of contractile units. Thus, the 60-fold (*S. pombe*) or 5-fold (*D. discoideum*) difference between the *in vivo* and *in vitro* speeds is vastly an underestimate of the real difference.

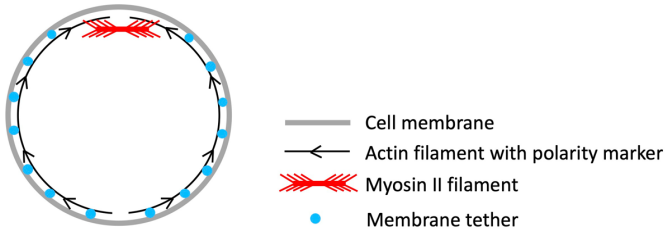

The second issue to be considered is the possible slowing of the actomyosin movement due to large load to contract CRs. Quantitative assessment of this possibility is difficult, but mutant *Dictyostelium* cells lacking myosin II on substrates can divide at a rate only 2-fold slower than the wild type cells (Zang et al., 1997), implying that at least in the case of adherent *Dictyostelium* cells, a very large force is not necessary to drive contraction of the CRs.

Based on these reasons, we speculate that contraction of the CR is regulated in an inhibitory manner in cells with and without a cell wall.

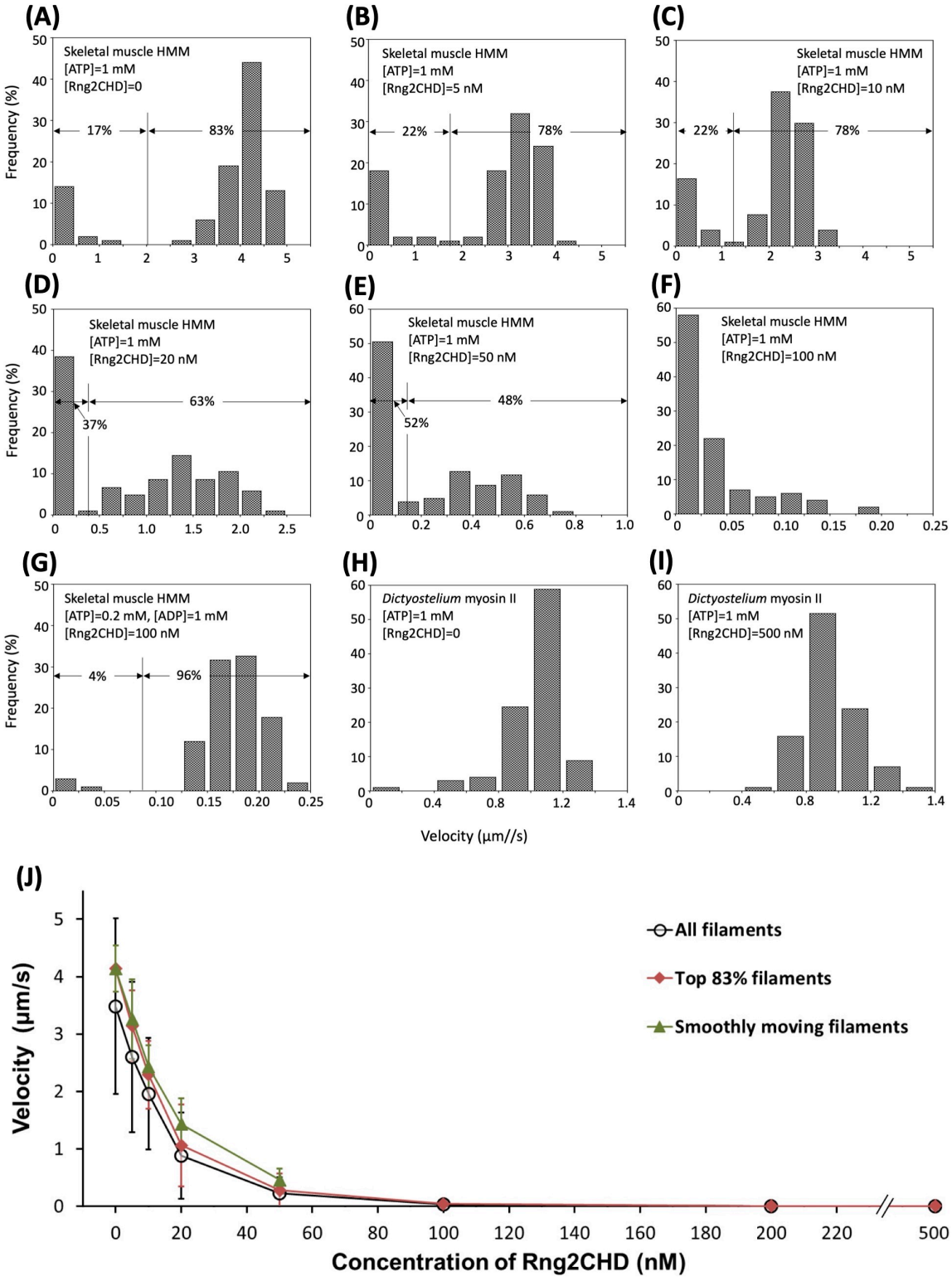

Figure Supplement 1. Detailed analyses on inhibition of actin-myosin II movements by Rng2CHD. Contaminating "bad" myosin heads that do not release actin filaments in the presence of

ATP would act as break and slow or stall the actin movements in *in vitro* motility assays. In the experiment shown in Figure 1A, a non-negligible fraction of the filaments were immobile in the absence of Rng2CHD. For the evaluation of motor activity of myosin *in vitro*, researchers often ignore those immobile filaments, visually select smoothly moving filaments and measure their velocities. This was not appropriate in this experiment, since Rng2CHD decreased the mean velocity by increasing the fraction of immobile filaments, in addition to slowing the smoothly moving filaments. This is the reason why we presented mean velocity of all actin filaments, including the immobile ones, under each experimental condition in Figure 1. In this Figure Supplement, we separately show contributions of the two effects, i.e., increase of the stalled filaments and slowing of the smoothly moving filaments, by Rng2CHD. In (**A-E**), distribution of velocities of all measured filaments are shown. In the absence of Rng2CHD, velocities on muscle HMM in the presence of 1 mM ATP had two distinct populations, one near zero, and the other centered around 4.1 μm/s. The fraction of the "immobile" filaments was 17%, and the faster one, which corresponds to smoothly moving filaments as judged by visual inspection of the traces, was 83%. The mean velocity of the immobile fraction was 0.22 ± 0.32 μm/s (mean ± SD, N=18), while that of the faster "smoothly moving" filaments was 4.1 ± 0.4 μm/s (N=83), with the mean velocity of all filaments of 3.5 ± 1.5 μm/s. Two distinct velocity distributions were recognizable up to the Rng2CHD concentration of 50 nM, when the fraction of the immobile filaments increased to 52% and the mean velocity of the smoothly moving filaments decreased to 0.46 ± 0.2 μm/s, with the mean velocity of all filaments of 0.23 ± 0.28 μm/s (**E**). At the Rng2CHD concentration of 100 nM or higher, the velocities of moving filaments became so slow that the distinction of two velocity fractions became impossible (**F**). Intriguingly, in the presence of 0.2 mM ATP and 1 mM ADP, most of the filaments were moving smoothly, albeit slowly, at 0.17 ± 0.04 μm/s even in the presence of 100 nM or 200 nM (not shown) Rng2CHD, with virtually no immobile filaments (4%) (**G**). Similarly, most of the filaments were moving smoothly on *Dictyostelium* myosin II, both in the absence (**H**) and presence of Rng2CHD (**I**). **J** shows mean ± SD actin velocities on muscle HMM in the presence of 1 mM ATP that were calculated by three different methods. Velocities of smoothly moving filaments were calculated up to the Rng2CHD concentration of 50 nM. The SDs are fairly large for all actin filaments (43% of the mean in the absence of Rng2CHD), but are reasonably small for smoothly moving filaments (10% of the mean). In the absence of Rng2CHD, 17% of the filaments were immobile, implying that immobile fraction in excess of 17% in the presence of Rng2CHD is due to the inhibitory effect of Rng2CHD. With this premise, we also calculated the mean velocities of the faster 83% filaments in each condition. This set of data may more accurately represent the overall inhibitory effect of Rng2CHD on motility by muscle HMM. Related to Figure 1.

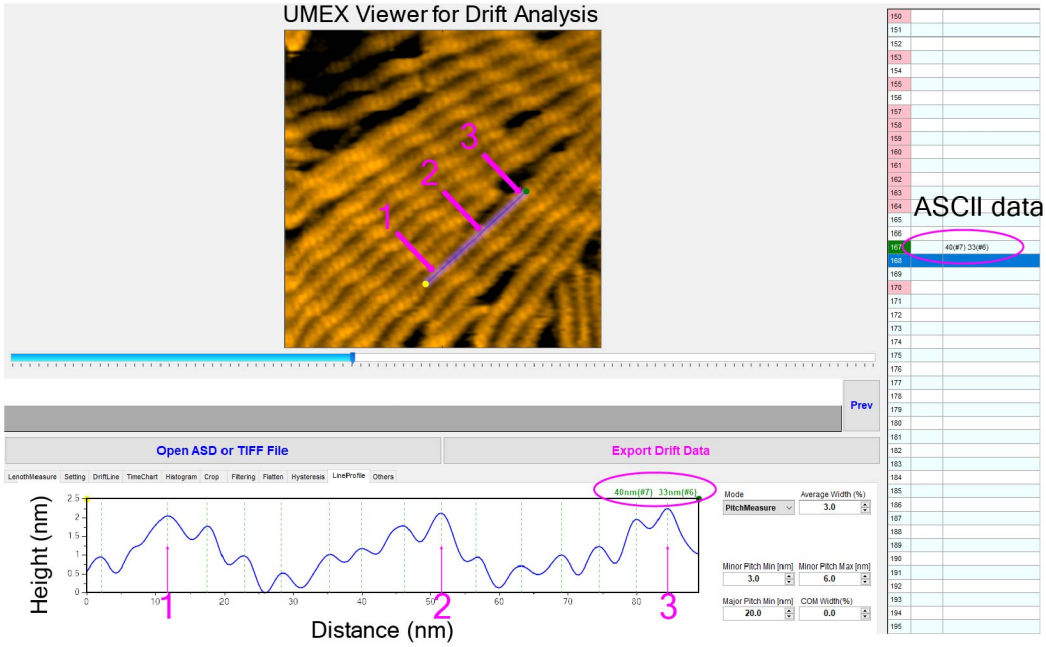

Figure Supplement 2. A screenshot demonstration of the peak determination and measurement of half helical pitch (HHP) of actin filaments using a semi-automated software UMEX Viewer for Drift Analysis. The typical threshold parameters were set to unambiguously determine the positions of actin protomers and measure HHPs along actin filaments, as described in detail in Materials and Methods. Magenta arrows denote the highest points (e.g., crossover points) automatically determined on a line drawn along an actin filament in the middle of the field (a major pitch min was set at 20 nm). Green dashed lines denote the positions of the highest points of individual actin protomers (the minor pitch min and max were set at 3 and 6 nm, respectively). For example, the two HHPs were measured between three adjacent purple arrows (peak 1, 2, 3) along an actin segment. The HHP and number of actin protomers counted per one HHP are shown simultaneously, as referred to the data marked by magenta oval. Typically, 20 – 30 actin filaments were selected and HHPs were measured for ~20 consecutive time frames. To minimize the measurement error of HHP, the straight actin segments were selected and the line profile (average width of 3%) was normally drawn to measure 1-3 consecutive half helices. Related to Figure 4.

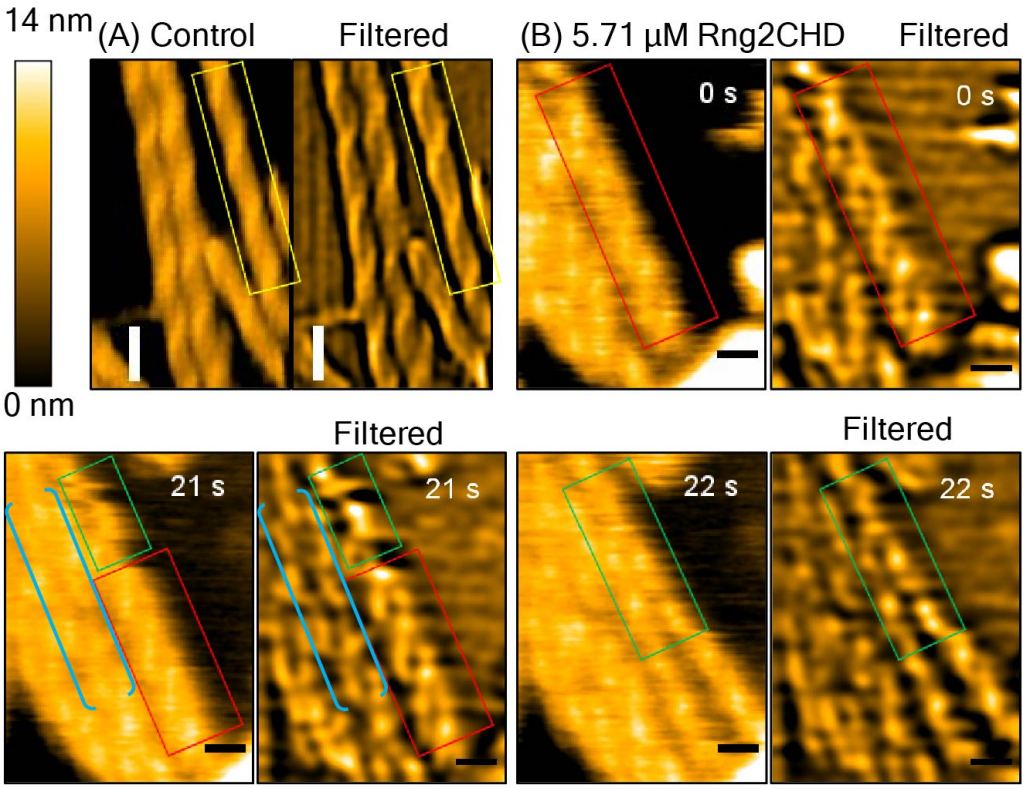

Figure Supplement 3. Distortion of helical structures of actin filaments and separation of protofilaments induced by high concentration of Rng2CHD. Control actin filaments (**A**) and actin filaments incubated with 5.7 µM Rng2CHD (**B**) were imaged by HS-AFM at different time points. Yellow rectangles denote control actin segments with compact and normal helical structures. Red rectangles denote actin filaments bound with Rng2CHD with abnormal helical structures. Green rectangles denote two single actin protofilaments separated from each other. Brackets denote actin segments that contain both abnormal helical structures and two separated protofilaments. Filtered AFM images were made to visualize more clearly helical structures of actin filaments by applying simultaneously Laplacian and Gaussian filters (sigma of 20). Bars: 25 nm. A stack of these images is shown in Video7. Related to Figure 4.

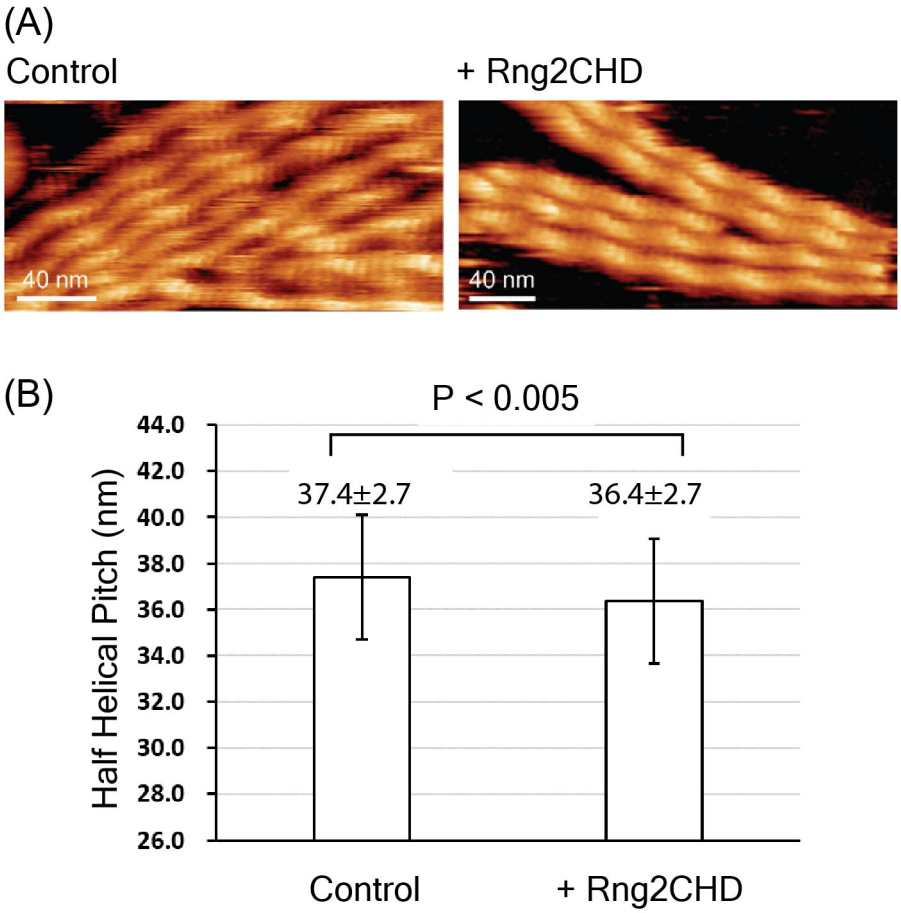

Figure Supplement 4. High-resolution AFM topography of actin subunits in control and Rng2CHD-treated actin filaments acquired by FM-AFM. (**A**) Typical high-resolution AFM topography image of actin subunits in control and Rng2CHD-treated filaments used for analyzing HHP. (**B**) Histogram of the HHP of control and Rng2CHD-treated actin filaments acquired by FM-AFM. Related to Figure 4.

Methods. We used a laboratory-built frequency modulation atomic force microscopy (FM-AFM) system operating in liquid environments equipped with an ultra-low noise cantilever deflection sensor (Fukuma et al., 2005; 2006). The photothermal excitation technique was used to drive the cantilever oscillation (Fukuma et al., 2012). AFM scanning was controlled by a commercial SPM controller (ARC2, Asylum Research, Santa Barbara, CA), and the oscillation amplitude of the cantilever was kept constant using a controller (OC4, SPECS, Berlin, Germany). AFM was operated in constant frequency shift Δf mode, where the tip-sample distance was adjusted such that Δf was kept constant. AFM data were acquired using an AFM cantilever (240AC-NG, OPUS, Sofia, Bulgaria) with nominal spring constants of 2 N/m and a nominal tip radius of ≤7 nm. After each measurement, the actual spring constant of each cantilever was determined using the thermal noise

method (Hutter et al., 1993). The obtained AFM images were processed by using WSXM or Gwyddion software.

G-actin was polymerized in FM-AFM buffer (40 mM KCl, 1 mM $MgCl_2$, 1 mM DTT, 0.5 mM EGTA, 1 mM ATP and 20 mM PIPES, pH 6.8) for 1 h at 22°C, and then 2.1 μM actin filaments were gently mixed with 0.32 μM Rng2CHD and incubated at room temperature for 5 to 10 min. Immediately, the control and Rng2CHD-treated actin filaments were deposited on a positively charged lipid bilayer (DPPC/DPTAP, 25/75 wt/wt) for 15 min, subsequently washed with 0.25x FM-AFM buffer 2 or 3 times prior to imaging in 0.25x FM-AFM buffer.

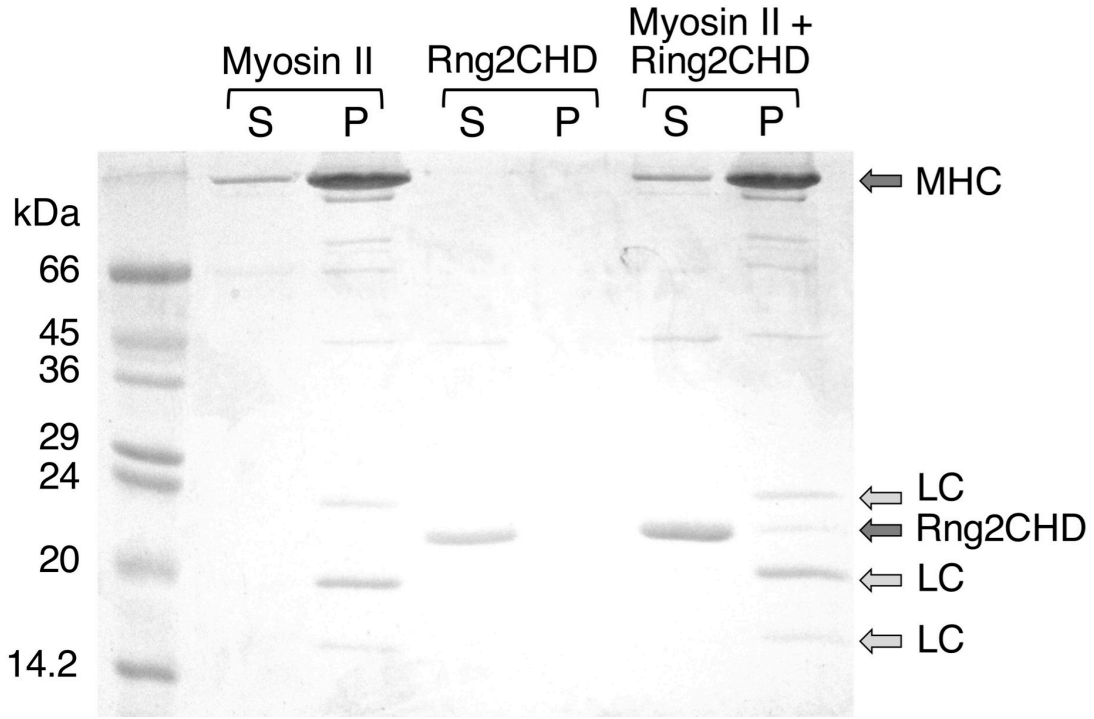

Figure Supplement 5. Co-sedimentation of Rng2CHD with skeletal muscle myosin II filaments. Skeletal muscle myosin II filaments, Rng2CHD and a mixture of the two proteins were centrifuged at 30,000 rpm for 10 min at 22°C in a Beckman TLA100.1 rotor, and the supernatant and pellet fractions were analyzed by SDS-PAGE. The concentration of myosin II and Rng2CHD was 2 μM, and the buffer was 10 mM Hepes pH 7.4, 25 mM KCl, 4 mM $MgCl_2$, 0.2 mM ATP and 1 mM DTT.

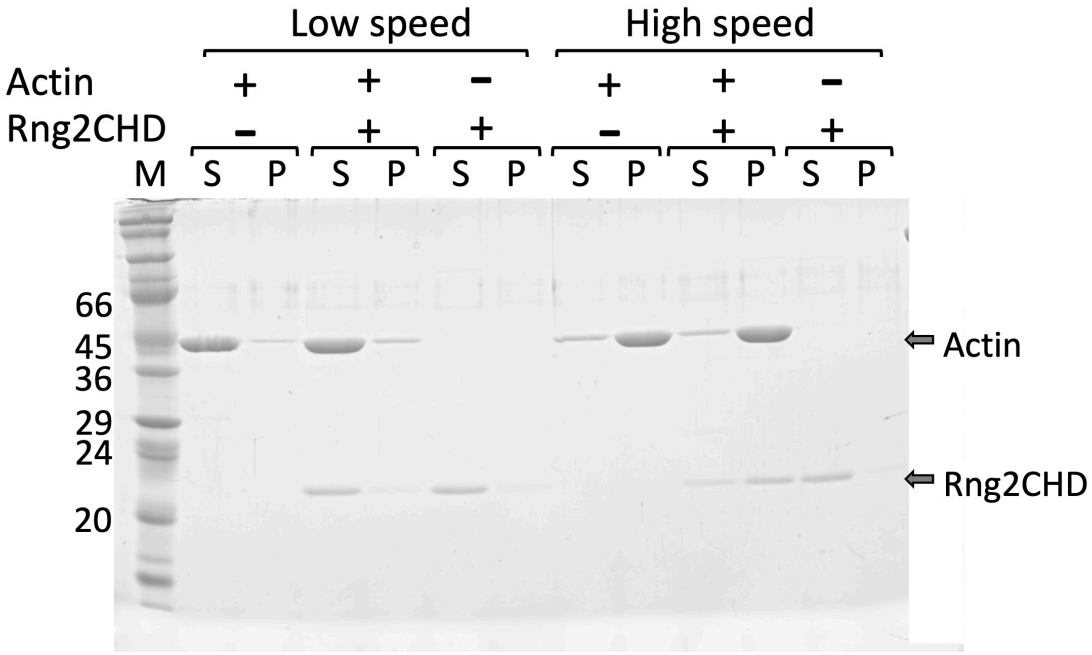

Figure Supplement 6. Co-sedimentation of Rng2CHD with actin filaments by low and high speed centrifugation.

Mixtures of 3 µM actin filaments and 1.5 µM Rng2CHD in KMEI (0.1 M KCl, 2 mM $MgCl_2$, 0.5 mM EGTA, 0.5 mM DTT, 0.2 mM ATP, and 10 mM imidazole, pH 7.5) were incubated for 1 h at 25°C. They were then centrifuged at 20,000 x *g* (low speed) for 15 min or at 200,000 x *g* (high speed) for 20 min, and pellet and supernatant fractions were analyzed by SDS-PAGE. Rng2CHD cosedimented with actin filaments after ultracentrifugation, but neither protein was pelleted by low speed centrifugation. Under the same condition, His-Rng2CHD–bundled actin filaments and both proteins were pelleted by low speed centrifugation (Takaine et al., 2009).

Table Supplement 1. Half helical pitch (HHP) of actin filaments incubated with different Rng2CHD concentrations at the equilibrium state (K_d of Rng2CHD = 0.92 μM). The value is a mean HHP ± SD. The differences between the mean HHP of control actin filaments (0 μM Rng2CHD) and those incubated with different Rng2CHD concentrations were statistically significant (*, p ≦ 0.001, two independent populations *t*-test). **Related to Figure 4**.

Actin (μM)	**Rng2CHD (μM)**	**HHP ± SD (nm)**	**Number of HHPs measured**	**t-test (*p*-value)**
0.59 (control)	0.0 (control)	36.4 ± 3.1	2225	
0.59	0.020	35.5 ± 2.9	1196	4.9×10^{-16}
0.59	0.25	35.0 ± 3.0	1026	4.4×10^{-31}
0.59	0.85	34.1 ± 4.0	1265	1.7×10^{-77}
0.59	2.6	34.2 ± 3.8	917	3.7×10^{-62}
0.59	5.7	34.2 ± 4.0	945	1.5×10^{-60}

1217 **References for Supplementary Materials**

1218 Furch M, Geeves MA, Manstein DJ. 1996. Modulation of Actin Affinity and Actomyosin Adenosine
1219 Triphosphatase by Charge Changes in the Myosin Motor Domain. *Biochemistry* **37**:6317–6326.
1220 Hutter J. Bechhoefer J. 1993. Determination of the spring constants of probes for force
1221 microscopy/spectroscopy. *J. Rev. Sci. Instrum* **64**: 1868-1873.
1222 Kron SJ, Spudich JA. 1986. Fluorescent actin filaments move on myosin fixed to a glass surface. *Proc*
1223 *Natl Acad Sci U S A* **83**:6272–6276. doi:10.1073/pnas.83.17.6272
1224 Lord M, Pollard TD. 2004. UCS protein Rng3p activates actin filament gliding by fission yeast myosin-
1225 II. *J Cell Biol* **167**:315–325. doi:10.1083/jcb.200404045
1226 Pelham RJ, Chang F. 2002. Actin dynamics in the contractile ring during cytokinesis in fission yeast.
1227 *Nature* **419**:82–86. doi:10.1038/nature00999
1228 Takaine M, Numata O, Nakano K. 2009. Fission yeast IQGAP arranges actin filaments into the
1229 cytokinetic contractile ring. *EMBO J* **28**:3117–3131. doi:10.1038/emboj.2009.252
1230 Warshaw DM, Desrosiers JM, Work SS, Trybus KM. 1990. Smooth muscle myosin cross-bridge
1231 interactions modulate actin filament sliding velocity in vitro. *J Cell Biol* **111**:453–463.
1232 doi:10.1083/jcb.111.2.453
1233 Zang JH, Cavet G, Sabry JH, Wagner P, Moores SL, Spudich JA. 1997. On the role of myosin-II in
1234 cytokinesis: division of *Dictyostelium* cells under adhesive and nonadhesive conditions. *Mol Biol*
1235 *Cell* **8**:2617–2629. doi:10.1091/mbc.8.12.2617
1236